STRONG COLLISIONS IN THE ELECTRON BROADENING OF SPECTRAL LINES FROM CHARGED RADIATORS IN HOT, DENSE PLASMAS

By

MARK ALLEN GUNDERSON

A DISSERTATION PRESENTED TO THE GRADUATE SCHOOL
OF THE UNIVERSITY OF FLORIDA IN PARTIAL FULFILLMENT
OF THE REQUIREMENTS FOR THE DEGREE OF
DOCTOR OF PHILOSOPHY

UNIVERSITY OF FLORIDA

2001

ACKNOWLEDGMENTS

I would like to acknowledge the continuous support, encouragement, and patience of Professor Charles F. Hooper, Jr. during the course of this research work and to thank him for suggesting this research topic. I would also like to gratefully acknowledge the support of Professor J. W. Dufty for his guidance through the course of this research, especially during the trying times of the last year. I would like to thank Dr. D. A. Haynes and Dr. G. C. Junkel-Vives for many helpful discussions and collaborations, without which this research would not be possible. Finally, I would like to thank my parents, Mr. and Mrs. Russell Gunderson, for providing support and encouragement throughout my education.

TABLE OF CONTENTS

Abstract of Dissertation Presented to the Graduate School
of the University of Florida in Partial Fulfillment of the
Requirements for the Degree of Doctor of Philosophy

STRONG COLLISIONS IN THE ELECTRON BROADENING OF SPECTRAL LINES FROM CHARGED RADIATORS IN HOT, DENSE PLASMAS

By

Mark Allen Gunderson

December 2001

Chairman: Charles F. Hooper, Jr.
Major Department: Physics

The model presented in this dissertation incorporates strong collision effects in the electron broadening of spectral lines from charged radiators in hot, dense plasmas. This model is an extension of an existing model, often referred to as the unified theory, that was originally developed to calculate frequency-dependent electron-broadening effects consistently from spectral line center to the far line wings for neutral hydrogen radiators and later adjusted for singly-charged helium radiators. Specifically, the extension allows for the consistent calculation of electron-broadening effects on line spectra emitted from mid-Z radiators (i.e., argon). This is accomplished through the use of relativistic radiator state data and also the inclusion of strong collision effects by incorporating, in addition to the dipole contribution, the effects of the monopole term and all other contributing higher-order "multipole" terms in the electron-radiator interaction. This model preserves the semiclassical treatment of the original model where the perturbing electrons move in classical trajectories and the radiator is treated through quantum mechanical means. It also preserves the calculation of the electron-broadening operator to all-orders in terms of the electron-radiator interaction.

Line spectra using the full-Coulomb, semiclassical, all-order electron-broadening model are compared to line spectra from a dipole-approximation version of this model. These line spectra are also compared to line spectra from full-Coulomb and dipole-approximation versions of a full quantum mechanical electron-broadening model expanded to second-order in a Born-like expansion in terms of the electron-radiator interaction. Significant shifts and distortions in the full-Coulomb line-shape calculations as compared to the dipole-approximation line-shape calculations at electron densities greater than $1 \times 10^{24}\,\mathrm{cm}^{-3}$ show that a dipole approximation of the electron-radiator interaction is no longer reasonable. Differences in the amount of shift and distortion in the comparisons of full-Coulomb calculations between the semiclassical, all-order and quantum mechanical, second-order models, specifically in the calculation of merging spectral lines at electron densities above $1 \times 10^{24}\,\mathrm{cm}^{-3}$, suggest that an all-order model is needed as the density increases.

CHAPTER 1
INTRODUCTION

When a radiating ion is immersed in a dense plasma, the energy levels of its bound states are modified by interactions with the surrounding ions and electrons. This results in spectral lines that are significantly broadened and shifted from the spectral lines of an isolated radiator [1,2]. The magnitude of this effect depends on the identity of the radiator and the density and temperature of the ions and electrons. Therefore, the width and shift of the lines provide a useful diagnostic measurement of the density and temperature of hot, dense plasmas [3–5]. As the density of a plasma increases, models describing the broadening and shifting of the spectra must be modified to more accurately account for high-density effects. This dissertation specifically examines the effects of strong electron collisions on the spectra of a radiator immersed in a plasma of ions and electrons and the potential use of the resulting spectra as a density and temperature diagnostic in the analysis of experimental data. A special focus is placed on plasma conditions in which some of the spectral lines begin to merge together.

It is appropriate at this point to parse the title of this work, as it contains some terms that need to be explained. In the context of this work, a "strong collision" refers to those collisions in which the strength of the interaction between the radiator and a perturbing electron is large enough and occurs over a sufficient period of time to disrupt a radiative transition from an upper state to a lower state. This work does not include the effects of ionizing collisions and electron capture. "Electron broadening" refers to the broadening effects of perturbing electrons through their modifications to the bound states of the radiator. "Charged radiators" corresponds to ions in the range of $6 \leq Z \leq 36$ that are undergoing radiative transitions and emitting spectra. "Hot, dense plasmas" refers to

nondegenerate plasmas where density broadening effects, specifically Stark broadening and electron broadening, are the dominant broadening mechanisms on the spectra and are large enough to cause spectral lines to overlap, or "merge", together.

Improvements in laser technology over the past 20 years led to the creation of plasmas with increasingly higher densities and temperatures [6–8]. To analyze and understand these plasmas, original theoretical line broadening models have been advanced and improved upon. Early models began with the Stark broadening of spectra from neutral radiators in the presence of an electric field from the distribution of the surrounding ions, commonly referred to as the ion microfield [9,10], along with an electron-broadening model utilizing a dipole interaction approximation. As the density and temperature of the plasmas increased, the study of spectra from ionic radiators became necessary [11–13] because the hydrogen atoms became completely ionized, thus requiring a multipole, or full-Coulomb calculation of the interaction between the charged radiator and the perturbing plasma electrons in the electron-broadening calculation [14,15]. The inclusion of the monopole term in the interaction led to the prediction of an experimentally noticeable red shift in the location of the spectral lines as the density of the plasmas increased [16–19]. This shift was shown to increase with increasing principal quantum number and electron density and to decrease with increasing temperature.

As a contextual aid for the model presented in this dissertation, we begin by briefly describing the experimental program currently underway to generate the experimental line spectra that are used to probe the plasma conditions achieved in the experiment through comparisons with theoretical line spectra from different models. In order to generate plasmas with the high electron densities needed to observe high-density effects, a high-powered laser, specifically the 64 beam OMEGA laser system at the Laboratory for Laser Energetics at the University of Rochester, is used to implode a small plastic shell (CH microballoon) filled with a gas consisting of deuterium with trace amounts of a mid-Z element (i.e., argon). The main variables of interest in our experiments include

the shell thickness of the CH microballoon, the microballoon's diameter, the pressure and composition of the fill gas, the laser beam pulse shape, and the total energy delivered on target.

For our most recently analyzed experiments through our NLUF (National Laser User Facility) campaign, the CH shell, or ablator, thickness generally was 20 microns, and the CH inner shell diameter was 940 microns. The composition and pressure of the fill gas ranged from 0.3% to 2% atomic fraction argon in 7-20 Atm of D_2. The laser-beam pulse shape was either a 1 ns ramp to 1 ns flat-top pulse or a 1 ns flat-top pulse. The total ultraviolet laser energy delivered on target was in the range of 19-24 kJ. The energy delivered on target would generally be a bit larger, but some total beam energy was sacrificed to achieve excellent beam balance of about $\Delta E/E \sim 3\%$ RMS. The experiments, with a few exceptions, were successful. The framing camera images and the static pinhole images all showed nearly circular core images, showing no significant excursions from a spherical implosion. Good argon K-shell data were observed in most of the experimental shots.

Our primary diagnostic was a streaked x-ray crystal spectrometer, or SSCA, operating with a flat RbAP (rubidium acid phthalate) crystal and an Au photocathode. The instrument provided approximately a 1.9 ns window with a resolution of 25 ps. The spectra were recorded on film and then digitized. Because the isolated line position is very important in determining important dense-plasma effects, including line shifts and line-merging effects, corrections for film sensitivity, filtering, photocathode response, streak-camera distortions including curvature of isotemporal lines and streak angle, and crystal/photocathode irregularities were performed on the data. Lineouts averaging over 25 ps were then extracted from the images, and the resulting time-dependent spectra exhibited time-varying Ar K-shell data. Spectral dispersion was determined using early-time lineouts when the electron density was small.

Our analysis of the data proceeds by performing a least squares (χ^2) fit to the spectral data using our group's fitting model. The model contains Stark broadened line shapes, NLTE population distributions, and corrections for the transfer of the thick alpha lines and the opacity of the diagnostic lines. The free parameters in our fitting model are the emissivity-averaged core electron temperatures and densities. This fitting process leads to an inference of time-dependent core conditions, something useful in its own right.

The fitting analysis of our most recently analyzed experiments confirmed that the experimental shots provided plasma conditions approaching those needed for our investigation of dense-plasma effects. We regularly reached densities just above 2×10^{24} cm^{-3}. At this density, high-density deviations from a linear Stark-broadening theory that does not include mixing between the upper-state manifolds of adjacent spectral series members, specifically in line merging behavior and strong-collision effects, are subtle. However, we saw indications in the data that a nonlinear Stark-broadening theory that includes mixing between the upper-state manifolds of adjacent series members yielded fits with a somewhat lower χ^2 than those from the linear theory, especially in the region of the Ly-γ line, as is shown in Figure 1.1. As our NLUF campaign progresses, we are confident that changes in the shell thickness, fill gas pressure, and pulse shape should give densities on the order of 4×10^{24} cm^{-3} where the differences are not so subtle.

As was just noted, we can currently generate electron densities of a magnitude such that strong collisions are beginning to affect the spectra from hydrogenic and helium-like argon. In other words, the spectra become sufficiently broad and shift to the extent that the contributions from strong collisions must be studied in greater detail. Previous models that limit the effects of strong collisions by including only those contributions to second-order in the perturbing electron-radiator interaction are valid over a range of $\Delta\omega \lesssim 2\omega_{plasma}$, where $\Delta\omega$ is the frequency separation from line center [20]. For example, with current electron densities, the Lyman-δ line of Argon broadens and shifts to the extent that it has already merged with the Lyman-γ line. In fact, the Lyman-$\gamma\delta$

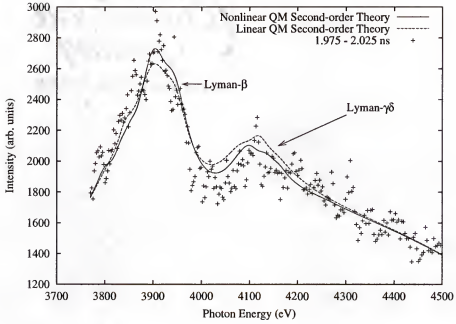

Figure 1.1: A comparison of theoretical fits of Ar^{+17} data from NLUF shot 22534 demonstrates that a quantum-mechanical nonlinear model to second-order in the full-Coulomb electron-radiator interaction gives a slightly better fit than the linear version of this model at an electron density of 1.9×10^{24} cm^{-3} and a temperature of 1.15 keV. The value of χ^2 is slightly smaller for the nonlinear fit.

spectral feature is already affecting the Lyman-β line significantly. In addition, these merged spectral features tend to be significantly broader than $2\omega_{plasma}$.

To incorporate strong collisions, as defined above, into the theoretical foundation of plasma line broadening for mid-Z ionic radiators, we develop an electron-broadening model similar to a model developed by Vidal, Cooper, and Smith (VCS) back in the late 1960s and early 1970s for neutral radiators [21–24], and extended a few years later by Greene and Cooper for ionized helium [25–27]. The VCS model was originally developed to calculate spectral lines of neutral hydrogen radiators from line center all the way out to the far line wing consistently. This model is sometimes referred to as the unified theory of line broadening because it consistently joined the impact model of line broadening that is appropriate around line center to the one-electron model of line broadening that is appropriate in the far wings of a line. The VCS model is a frequency-dependent, binary-collision electron-broadening model that includes terms to all-order

in the interaction between the radiator and the perturbing electron through the calculation of a time development operator. It is a semiclassical model, meaning that it treats the perturbing electrons as classical particles using classical trajectories while treating the radiator through quantum mechanical means. Because the VCS model focuses on low-Z neutral radiators and excludes strong-collision contributions, this model uses only the dipole term in the perturbing electron-radiator interaction and uses nonrelativistic wavefunctions to describe the radiator states. A no-quenching approximation is also applied in the VCS model so that perturbations on the radiator do not induce non-radiative transitions between the initial and final states. Electron correlations in this model are included by considering only those perturbing electron-radiator interactions which occur within a sphere about the radiator with a radius of the Debye length. Any electrons outside of this sphere do not interact with the radiator because the radiator is effectively screened by the electrons within the Debye sphere.

The difference between the VCS model and the model as modified by Greene and Cooper was to replace the straight-line trajectories of the perturbing electrons for neutral radiators with hyperbolic trajectories for charged radiators. The other aspects of the model basically remained unchanged. It is this version of the VCS model modified for charged low-Z radiators that is similar to the model developed in this dissertation.

In order to calculate theoretical spectra for higher-Z radiators (i.e., Argon) and to include contributions from strong collisions, the model presented in this work differs from the VCS charged-radiator model in these important ways:

- The interaction between the perturbing electron and the radiator is calculated using a multipole, or full-Coulomb calculation.
- Relativistic wavefunctions and the corresponding energy level structure from a relativistic atomic physics package are employed to describe the atomic physics of mid-Z radiators.
- A minimum separation cutoff is incorporated into the model. This cutoff is the Landau length modified by the radiator charge and quantum diffraction effects. The cutoff corrects for the singularity caused by the treatment of the electrons as classical particles.

- The distribution function is generalized to provide temperature-dependent changes in the relative populations of the radiator states modified by the interaction between the perturbing electron and the radiator.
- The no-quenching approximation, which prohibits nonradiative transitions caused by perturbations between states of differing principle quantum number n, must be relaxed to allow for nonradiative transitions between upper states of spectral lines which are beginning to merge together.

With these improvements, this model is able to accurately calculate isolated and merging spectral lines from mid-Z radiators.

In addition to the calculation of isolated and merging spectral lines, there are several other applications for this model. Differences in merged spectral lines at higher electron densities due to strong-collision effects from the higher-order terms has the possibility of altering what we perceive as the distinction between continuum and bound states. Because ionization balance is sensitive to any changes in the energy level structure [28–30] and opacity is sensitive to the energy location and intensity of line emission, an understanding of the effects of strong collisions on the merged composite spectral features that lie near the continuum edge can be important.

Even at lower densities, the wings of a line profile are significantly dependent on the effects of strong collisions through the higher-order terms. This can have significant effects on Rosseland group opacities [31]. They are very sensitive to changes in the intensity of the line profile in the wings because they are proportional to a harmonic mean of the absorption coefficient. Rosseland group opacities, in turn, are important in the calculation of multi-group diffusion radiative transfer effects. These effects, which are important in determining the amount of radiation that passes through different portions of the frqequency spectrum, can be of importance in both astrophysical studies and in fusion research.

To outline this dissertation, in Chapter 2, we present a model of spectral line broadening for radiators immersed in hot, dense plasmas. We consider several broadening mechanisms:

- Doppler broadening due to thermal motion of the radiator is included.
- Stark broadening due to the distribution of static-ion fields is included.
- Dynamical ion broadening due to transitions between the static-ion fields is included.
- Electron broadening due to strong electron-radiator collisions is included.

For the plasma conditions under consideration, the dominate broadening mechanisms are the Stark broadening due to the distribution of static-ion fields and the electron broadening due to electron-radiator collisions. The relative importance of these broadening mechanisms are discussed in detail by others [18], and is not revisited here. Some simplifying assumptions are made for calculational reasons which will need to be further investigated in the future.

Chapter 3 focuses on the calculation of the electron-broadening, or width-and-shift, operator. We introduce a convenient form for the electron-radiator interaction, discuss the classical-path approximation, and apply some approximations to allow for tractable calculations of this operator.

In Chapter 4, we discuss the details of the calculation of spectral features. We then provide an analysis of widths and shifts due to electron broadening. We also show comparisons of line shapes using the electron-broadening model described in Chapter 3 with line shapes utilizing different electron-broadening models. Finally, we look at comparisons of results from calculations involving the merging of spectral lines.

In the Conclusions, we summarize our findings and consider the effects of the treatment of strong electron collisions in our model on other areas in the field of dense plasma physics.

CHAPTER 2
LINE BROADENING IN HOT DENSE PLASMAS

The first step in considering line broadening in hot, dense plasmas is to develop a model describing the plasma. This model is crucial to an understanding of how the interactions of the plasma with a highly ionized radiator affects the spectral lines emitted by the radiator.

The radiators (i.e., argon) are assumed to be well separated in the plasma and do not interact with each other. Thus, the plasma is broken up into noninteracting cells where each cell contains one radiator along with electrons and ions that perturb the quantum states of the radiator. It is from within this perturbing plasma environment that the radiator emits its radiation. The frequency-dependent power distribution of the radiation, specifically electric dipole radiation, can be written in terms of an ensemble average over all the possible states of radiator together with the plasma environment as [1,2]

$$P(\omega) = \frac{4\omega^4}{3c^3} \sum_{a,\,b} |\langle b|\, \boldsymbol{d}\, e^{-i\boldsymbol{k}\cdot\boldsymbol{r}} |\, a\rangle|^2 \rho_a \delta(\omega - \omega_{ab}) \tag{2.1}$$

where a represents an initial state of the radiator and plasma environment, weighted by the corresponding eigenvalue of the density matrix ρ_a, b represents a final state of the radiator and plasma environment, and $\hbar\omega_{ab}$ is the energy of the transition. The electric dipole operator of the system is denoted by $\boldsymbol{d}$, the vector $\boldsymbol{k}$ represents the wave vector of the emitted radiation, and $\boldsymbol{r}$ is the center of mass position of the radiator.

Because ω^4 does not vary significantly over the frequency range of the spectra of interest, the line shape is defined from the power distribution formula as

$$I(\omega) = \sum_{a,\,b} \langle a|\, e^{i\boldsymbol{k}\cdot\boldsymbol{r}} \boldsymbol{d} |\, b\rangle \cdot \langle b|\, \boldsymbol{d}\, e^{-i\boldsymbol{k}\cdot\boldsymbol{r}} |\, a\rangle \rho_a \delta(\omega - \omega_{ab})\,. \tag{2.2}$$

Using the definitions

$$\hbar\omega_{ab} = E_a - E_b \quad \text{and} \quad \boldsymbol{d}_{\boldsymbol{k}} = \boldsymbol{d}\, e^{-i\boldsymbol{k}\cdot\boldsymbol{r}} \tag{2.3}$$

and the integral representation of the Dirac delta function, the line shape can be rewritten in the form

$$I(\omega) = \frac{1}{2\pi}\int_{-\infty}^{\infty} \mathrm{d}t\; e^{\mathrm{i}(\omega-\mathrm{i}\epsilon)t}\,\mathrm{Tr}\{\boldsymbol{d}_{\boldsymbol{k}}\cdot e^{-\mathrm{i}Ht/\hbar}\rho\boldsymbol{d}_{\boldsymbol{k}}^{\dagger}e^{iHt/\hbar}\} \tag{2.4}$$

where the trace is over the plasma-radiator system. The expression inside the trace is the autocorrelation function of the radiator dipole, keeping in mind that the trace is invariant over cyclic permutations. The damping factor ϵ in the transform represents the natural line width which corresponds to the lifetime of the upper state of the transition. The density matrix operator has the form

$$\rho = \frac{\exp(-H/k_BT)}{\mathrm{Tr}\{\exp(-H/k_BT)\}}. \tag{2.5}$$

To complete the definition of the line shape function, the form of the Hamiltonian H must be specified. Separating out the important interactions in the plasma-radiator system, H has the form

$$H = H_r^{cm} + H_r^{int} + H_i + H_e + V_{i,e} + V_{i,r} + V_{e,r}\,. \tag{2.6}$$

The first term refers to the center-of-mass motion of the radiator while the second term refers to the internal states of the radiator. The next two terms refer to the sum of the kinetic energies and the interactions within the respective subsystem, or

$$H_i = K_i + V_{i,i} \quad \text{and} \quad H_e = K_e + V_{e,e}\,. \tag{2.7}$$

The last three terms represent the interactions between the radiator, the electrons, and the ions.

Now that we have the starting expression for the line shape, we can make certain approximations based on the properties of the plasmas considered. Because these hot plasmas have a radiator (i.e., argon) that is usually much more massive then the perturbing ions (i.e., deuterium) and obviously much more massive then the electrons, it is usually appropriate to assume that the center-of-mass motion of the radiator is statistically independent from the other degrees of freedom [32–34]. Stated another way, the impulse imparted to the radiator from the electron and ion perturbations is small relative to the magnitude of the radiator's momentum over the lifetime of the upper state of the transition. Assuming that the radiators are well separated and can be treated as an ideal gas, the line shape can be expressed as a convolution of a Doppler profile (gaussian) and a Stark-broadened line shape in the radiator center-of-mass frame [35,36]

$$I(\omega) = \frac{1}{\sqrt{2\pi}\sigma} \int_{-\infty}^{\infty} \mathrm{d}\omega' \exp\left(-\frac{(\omega-\omega')^2}{2\sigma^2}\right) I_{CM}(\omega') \tag{2.8}$$

where

$$2\sigma^2 = \frac{\omega'^2}{c^2}\left(\frac{2k_BT}{m_r}\right). \tag{2.9}$$

The line shape in the radiator center-of-mass frame is given by

$$I_{CM}(\omega) = \frac{1}{2\pi}\int_{-\infty}^{\infty} \mathrm{d}t\ e^{\mathrm{i}(\omega-\mathrm{i}\epsilon)t}\,\mathrm{Tr}\{\boldsymbol{d}\cdot e^{-\mathrm{i}H't/\hbar}\rho'\boldsymbol{d}^{\dagger}e^{\mathrm{i}H't/\hbar}\} \tag{2.10}$$

where the density matrix operator now has the form

$$\rho' = \frac{\exp(-H'/k_BT)}{\mathrm{Tr}\{\exp(-H'/k_BT)\}} \tag{2.11}$$

with the Hamiltonian given by

$$H' = H_r^{int} + H_i + H_e + V_{i,e} + V_{i,r} + V_{e,r} \,. \tag{2.12}$$

To keep the notation simple, we drop the internal state indicator on the isolated radiator Hamiltonian.

The center-of-mass line shape can be simplified by taking advantage of the fact that the expression inside the trace is the autocorrelation function of the electric radiator dipole, $C(t)$. Because $\boldsymbol{d}$ is hermitian, $C(t)$ has the property

$$C(-t) = C(t)^* \tag{2.13}$$

that can be employed to write the line shape as

$$I_{CM}(\omega) = \frac{1}{\pi}\Re \int_0^\infty \mathrm{d}t \; e^{i(\omega - i\epsilon)t} \, \mathrm{Tr}_{r,p}\{\boldsymbol{d} \cdot e^{-iH't/\hbar}\rho' \boldsymbol{d} e^{iH't/\hbar}\} \,. \tag{2.14}$$

From this point on, the center-of-mass notation on the Stark-broadened line shape function is suppressed. The notation $I(\omega)$ represents the Stark-broadened center-of-mass line shape.

As a lead in to the simplification of the line shape expression, it is convenient to regroup the terms of the Hamiltonian in the form

$$H' = H_r + H_i' + H_e' + V_{i,e} + V_{i,r}^{(1)} + V_{e,r}^{(1)} \tag{2.15}$$

where the ion Hamiltonian is given by

$$H_i' = K_i + V_{i,i} + V_{i,r}^{(0)} \tag{2.16}$$

and the electron Hamiltonian is given by

$$H_e' = K_e + V_{e,e} + V_{e,r}^{(0)}. \tag{2.17}$$

Note that the monopole, or point-charge, interactions between the radiator and the perturbing ions and electrons, which are denoted by the superscript " 0 ", have been separated out and combined with the ion and electron portions of the Hamiltonian, respectively. Thus, the dynamical behavior of the ions and electrons in the given radiator cell of the plasma is defined in the presence of the charge of the radiator. Due to the repulsion between the charged radiator and the perturbing ions, it should be a reasonable approximation that the ions do not penetrate the the orbitals of the radiator. The remainder of the ion-radiator interaction $V_{i,r}^{(1)}$ can be approximated by a radiator dipole interaction with the electric field due to the ions

$$V_{i,r}^{(1)} = V_{i,r}^{(1)}(\boldsymbol{E}_i) = \boldsymbol{d} \cdot \boldsymbol{E}_i \,. \tag{2.18}$$

The effects of the higher-order terms of $V_{i,r}^{(1)}$ on various line shapes have been evaluated [37] and appear to have a relatively small effect in comparison to the effects of plasma-induced line shifts on the line shapes. The term $V_{e,r}^{(1)}$ now consists of the interaction of the radiator with the perturbing electrons excluding the point-charge monopole interaction. In other words, this term represents the interaction of the perturbing electrons with the internal electronic structure of the radiator.

Even without correlations between Doppler broadening and Stark broadening in the line shape expression, the calculation of the Stark-broadened center-of-mass line shape function is still very complicated. A method to simplify the calculation of the line shape function is employed by integrating the line shape at a specific value of the static-ion

field over a distribution of static-ion fields

$$I(\omega) = \int \mathrm{d}\epsilon\, Q(\epsilon) J(\omega, \epsilon) \tag{2.19}$$

where

$$Q(\epsilon) = \mathrm{Tr}_i\{\rho_i \delta(\epsilon - \boldsymbol{E}_{si})\} \tag{2.20}$$

is the probability that the distribution of ions around the radiator results in an electric field (microfield) of the value ϵ at the location of the radiator. The functional form of the probability distribution function is shown in Figure 2.1 for various temperatures and densities. The electron-broadened line shape evaluated at a given value of the static-ion microfield, $J(\omega, \epsilon)$, is given by

$$J(\omega, \epsilon) = -\frac{1}{\pi} \Im\, \mathrm{Tr}_r\{\boldsymbol{d} \cdot \boldsymbol{D}(\omega, \epsilon)\} \tag{2.21}$$

and its functional form is shown in Figure 2.2. The details of the computation of $Q(\epsilon)$ and $J(\omega, \epsilon)$ are described at the beginning of Chapter 4. A comparison of these expressions to equation 2.14 shows that $\boldsymbol{D}(\omega, \epsilon)$ has the form

$$\boldsymbol{D}(\omega, \epsilon) = \frac{1}{Q(\epsilon)} \int_0^\infty \mathrm{d}t\; e^{\mathrm{i}(\omega - \mathrm{i}\epsilon)t}\, Tr_p \left\{ \delta\left(\epsilon - \boldsymbol{E}_{si}\right) \rho'\, e^{-\mathrm{i}H't/\hbar} \boldsymbol{d}\, e^{\mathrm{i}H't/\hbar} \right\} \tag{2.22}$$

where the distribution function of the plasma-radiator system ρ' commutes with the time evolution operator of the plasma-radiator system $e^{-\mathrm{i}H't/\hbar}$.

The next step in the calculation of the line shape expression involves the derivation of the equation of motion for $\boldsymbol{D}(\omega, \epsilon)$ along with the derivation of its solution. The details of this derivation are given in Appendix A, and the resulting equation of motion

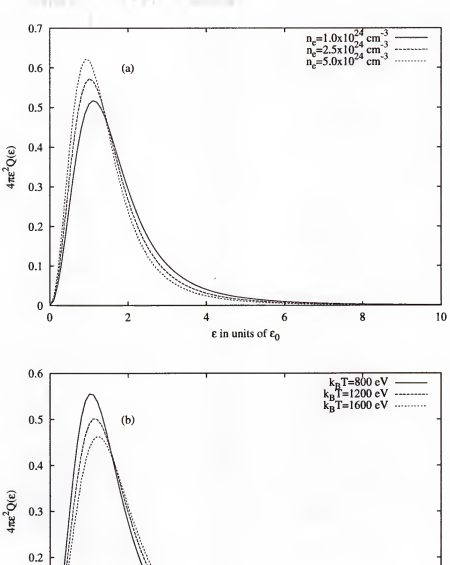

Figure 2.1: Microfield probability distribution functions $4\pi\epsilon^2 Q(\boldsymbol{\epsilon})$ are shown for 1% atomic fraction argon in D_2. The microfield is given in units of $\epsilon_0 = e^2/r_0$ where r_0 is the inter-electron spacing. a) The density behavior of $4\pi\epsilon^2 Q(\boldsymbol{\epsilon})$ is shown at a temperature of 1 keV. Note that the most probable field value increases with n_e keeping in mind the density dependence of the reduced units. b) The temperature behavior of $4\pi\epsilon^2 Q(\boldsymbol{\epsilon})$ is shown at a density of 1×10^{24} cm^{-3}. Note that the most probable field value increase with temperature as well.

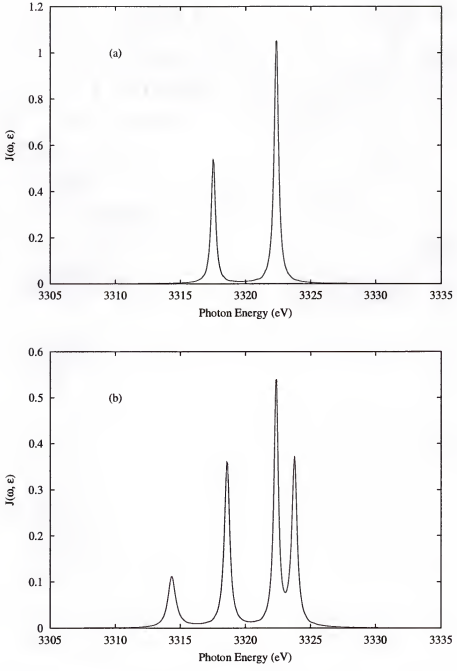

Figure 2.2: $J(\omega, \epsilon)$ is shown for the Lyman-α line of Ar^{+17} at a density of 1×10^{24} cm^{-3} and a temperature of 1 keV. Field values are given in units of $\epsilon_0 = e^2/r_0$ where r_0 is the inter-electron spacing. a) This profile is calculated using the field value $\epsilon = 0$. Thus, there is no ion Stark splitting. b) This profile is calculated using the field value $\epsilon = 1.1$, the most probable field for these plasma conditions.

has the form

$$\left[\omega - L_r - L_{i,r}^{(1)}(\epsilon) - B_\epsilon(\epsilon) - M_\epsilon(\omega,\epsilon)\right] \boldsymbol{D}(\omega,\epsilon) - \int \mathrm{d}\epsilon' M_i(\epsilon,\epsilon';\omega)\boldsymbol{D}(\omega,\epsilon') = \rho_{\epsilon,r}\boldsymbol{d} \qquad (2.23)$$

where we have assumed that there are no dynamical correlations between the electrons and the ions. The broadening contribution from the isolated radiator operator L_r is given by

$$L_r \boldsymbol{D}(\omega,\epsilon) = \frac{1}{\hbar}[H_r, \boldsymbol{D}(\omega,\epsilon)] \qquad (2.24)$$

and the broadening contribution from the partial removal of the degeneracy of the radiator states in the manifold of the n^{th} principal quantum number due to the presence of an ion microfield (ion Stark splitting) is given by

$$L_{i,r}^{(1)}(\epsilon)\boldsymbol{D}(\omega,\epsilon) = \frac{1}{\hbar}[\boldsymbol{d}\cdot\boldsymbol{\epsilon}, \boldsymbol{D}(\omega,\epsilon)]\,. \qquad (2.25)$$

The operator $M_i(\epsilon,\epsilon';\omega)$ describes the effects of the motion of the perturbing ions on the radiator dipole through fluctuations in the ion microfield [38]. Using an ion motion assumption in which the transitions among different field values are instantaneous and uncorrelated (Poisson process), the ion-dynamics collision term can be written in the form

$$\begin{aligned}\int \mathrm{d}\epsilon' M_i(\epsilon,\epsilon';\omega)\boldsymbol{D}(\omega,\epsilon') &= \mathrm{i}\nu\rho_{\epsilon,r}\int \mathrm{d}\epsilon' Q(\epsilon')\left\{\rho_{\epsilon,r}^{-1}\boldsymbol{D}(\omega,\epsilon) - \rho_{\epsilon',r}^{-1}\boldsymbol{D}(\omega,\epsilon')\right\} \\ &= \mathrm{i}\nu\boldsymbol{D}(\omega,\epsilon) - \mathrm{i}\nu\rho_{\epsilon,r}\int \mathrm{d}\epsilon' Q(\epsilon')\rho_{\epsilon',r}^{-1}\boldsymbol{D}(\omega,\epsilon') \qquad (2.26)\end{aligned}$$

where ν is directly proportional to the momentum autocorrelation function of the ions and is a measure of the importance of ion motion effects on the line shape. Utilizing this form of the ion-dynamics collision term, the operator $\boldsymbol{D}(\omega,\epsilon)$ can be shown to have

the form

$$D(\omega,\boldsymbol{\epsilon}) = G(\omega,\boldsymbol{\epsilon})\,\frac{1}{1+\mathrm{i}\nu\int \mathrm{d}\boldsymbol{\epsilon}'\,Q(\boldsymbol{\epsilon}')G(\omega,\boldsymbol{\epsilon}')}\,\rho_{\boldsymbol{\epsilon},r}\,\boldsymbol{d} \tag{2.27}$$

where

$$G(\omega,\boldsymbol{\epsilon}) = \frac{1}{\omega - L_r - L_{i,r}^{(1)}(\boldsymbol{\epsilon}) - B_e(\boldsymbol{\epsilon}) - M_e(\omega,\boldsymbol{\epsilon}) - \mathrm{i}\nu} \tag{2.28}$$

and the distribution function has the form

$$\rho_{\boldsymbol{\epsilon},r} = \frac{e^{-[H_r + \boldsymbol{d}\cdot\boldsymbol{\epsilon}]/k_B T}}{\mathrm{Tr}_r\{e^{-[H_r+\boldsymbol{d}\cdot\boldsymbol{\epsilon}]/k_B T}\}}\,. \tag{2.29}$$

Finally, we arrive at the main topic of this dissertation: the electron-broadening effects of the perturbing plasma electrons. The effects of plasma electron perturbations on the radiator dipole moment are contained in the static part $B_e(\boldsymbol{\epsilon})$ and the dynamic part $M_e(\omega,\boldsymbol{\epsilon})$ of the electron-broadening, or width-and-shift operator. The approximation that there are no dynamical correlations between the electrons and the ions is reasonable because the ions are much heavier and slower than the electrons and thus interact with the radiator dipole over a time scale much longer than the time scale of the interaction of the electrons with the radiator dipole. The electrons affect the ion broadening only through the screened ion field $\boldsymbol{E}_{si}$. The width-and-shift operator, when expanded out in a series, has the form of a Born expansion in the electron-radiator interaction $V_{e,r}^{(1)}$. With the substitution $V_{e,r}^{(1)} \rightarrow \lambda V_{e,r}^{(1)}$, the expansion has the form

$$M_e'(\omega,\boldsymbol{\epsilon}) = \sum_{n=1}^{\infty} \lambda^n \{B^{(n)}(\boldsymbol{\epsilon}) + M_e^{(n)}(\omega,\boldsymbol{\epsilon})\} \tag{2.30}$$

where n defines the term to n^{th} order in the interaction. To see the form of the general width-and-shift operator, look at Equations B.1 and B.2 in Appendix B.

In order to work with a numerically tractable form of the dynamic part of the width-and-shift operator, $M_e'(\omega,\boldsymbol{\epsilon})$, a few approximations must be made. These approximations are discussed in detail in Appendix B. The first is the one-electron approximation,

where only one strong electron collision is allowed with the radiator at a time. As a result of this approximation, correlations between plasma electrons have been neglected. Therefore, the screening effects of electron correlations on the electron-radiator interaction are approximated with a static Debye screening model [39], or in other words, interactions between the radiator and the perturbing electron are considered only when the electron enters a sphere with a radius of the Debye length centered around the radiator.

Next, we apply the no-quenching approximation where no perturbation-induced non-radiative transitions are allowed between upper and lower states. From Equation 2.27, it is observed that the width-and-shift operator acts on the radiator dipole moment $\boldsymbol{d}$. Under the no-quenching approximation, only matrix elements between initial and final states of the radiator transition for this occurrence of the radiator dipole moment, noted by $\boldsymbol{d}_{if}$, are allowed in the line shape expression, and the matrix elements of the electron-radiator interaction between initial and final states of the transition are zero. This approximation leads to four separate terms in the width-and-shift operator as is seen in Equation B.17. The first term describes the broadening on the upper states of the transition, the last term describes the broadening on the lower states of the transition, and the two intermediate terms are interference terms between upper and lower states. Because the results shown in this work consist of line spectra which have no significant lower-state broadening, we apply a no lower-state broadening approximation where we concentrate specifically on the first term that includes the effects of upper-state broadening.

With these approximations, the first term of the static part of the width-and-shift operator has the form

$$B^{first}(\epsilon)\boldsymbol{d}_{if} = n_e \mathrm{Tr}_{1e}\{V^{(1)}_{1e,r}\,\rho_{1e,\epsilon,r}\}\,\rho^{-1}_{\epsilon,r}\boldsymbol{d}_{if} \tag{2.31}$$

and the first term of the dynamic part of the width-and-shift operator has the form

$$M^{first}(\omega,\epsilon)\boldsymbol{d}_{if} = -in_e \int_0^\infty \mathrm{d}t\, e^{\mathrm{i}(\omega - H_{\epsilon,r}+\mathrm{i}\epsilon)t}\, \mathrm{Tr}_{1e}\left\{ \tilde{V}^{(1)}_{1e,r}(t)\, U(t,0) \right. \\ \left. \cdot \rho_{1e,\epsilon_r}\, V^{(1)}_{1e,r}\, \rho^{-1}_{\epsilon,r}\, \boldsymbol{d}_{if}\, U^\dagger(t,0) \right\} e^{\mathrm{i}H_{\epsilon,r}t}\,. \tag{2.32}$$

The time development operator has the form

$$U(t,0) = \vartheta \exp\left\{ -\mathrm{i} \int_0^t \mathrm{d}t'\, \tilde{V}^{(1)}_{1e,r}(t') \right\} \tag{2.33}$$

where ϑ indicates a time-ordered calculation of the exponential term,

$$\tilde{V}^{(1)}_{1e,r}(t) = e^{\mathrm{i}(H_{\epsilon,r}+H'_{1e})t}\, V^{(1)}_{1e,r}\, e^{-\mathrm{i}(H_{\epsilon,r}+H'_{1e})t} \tag{2.34}$$

is the perturbing electron-radiator interaction in the interaction representation, and

$$H_{\epsilon,r} = H_r + \boldsymbol{d}\cdot\boldsymbol{\epsilon}\,. \tag{2.35}$$

The time development operator satisfies the differential equation

$$\mathrm{i}\hbar \frac{\partial U(t,0)}{\partial t} = \tilde{V}^{(1)}_{1e,r}(t) U(t,0)\,. \tag{2.36}$$

Because of the no-quenching approximation, operators to the left of $\boldsymbol{d}_{if}$ act on the initial-state manifold of the transition and operators to the right of $\boldsymbol{d}_{if}$ act on the final-state manifold of the transition.

The form of the Hamiltonian that now defines the line broadening problem as presented here is given by

$$H = H_{\epsilon,r} + H'_{1e} + V^{(1)}_{1e,r}\,. \tag{2.37}$$

Note that the monopole term of the ion-radiator interaction, screened by the plasma electrons, has been incorporated into the calculation of the ion electric microfield. The remainder of the ion-radiator interaction is approximated solely by the dipole term of the interaction that depends on the internal state of the radiator and the ion microfield. The plasma electrons, in the presence of a charged radiator, are described by the plasma electron Hamiltonian and the monopole term of the interaction between the perturbing electron and radiator charge

$$H'_{1e} = K_{1e} + V^{(0)}_{1e,r} \tag{2.38}$$

and the effects of electron correlations $V_{e,e}$ are approximated using the static Debye screening approach mentioned earlier.

In summary, the model constructed to describe plasma broadened line shapes include these broadening mechanisms:

- Doppler broadening due to thermal motion of the radiator is included.
- Stark broadening due to the distribution of static-ion fields is included.
- Dynamical ion broadening due to transitions between the static-ion fields is included.
- Electron broadening due to strong electron-radiator collisions is included.

In the next chapter, a detailed discussion of the width-and-shift operator including the effects of strong collisions is given. A classical path treatment is imposed on the perturbing electrons, and a full-Coulomb treatment of the electron-radiator interaction is employed.

CHAPTER 3
ELECTRON-BROADENING MODEL

In this chapter, the electron width-and-shift operator $M'(\omega, \boldsymbol{\epsilon})$ is discussed in more detail. We begin with a discussion of the electron-radiator interaction used in the calculation of $M'(\omega, \boldsymbol{\epsilon})$. A classical-path approximation is applied to the perturbing plasma electrons, and the final calculational form of the width-and-shift operator is presented.

3.1 Electron-Radiator Interaction

The Hamiltonian associated with line broadening as shown in Chapter 2 has the form

$$H = H_r + H'_{1e} + \boldsymbol{d} \cdot \boldsymbol{\epsilon} + V^{(1)}_{1e,r} \tag{3.1}$$

where H_r is the isolated radiator Hamiltonian, H'_{1e} is the plasma electron Hamiltonian in the presence of the monopole term of the electron-radiator interaction, $\boldsymbol{d} \cdot \boldsymbol{\epsilon}$ defines the Stark splitting of the radiator levels, and $V^{(1)}_{1e,r}$ gives the interaction of the perturbing electron with the internal electronic structure of the radiator. The monopole term of the electron-radiator interaction has the form

$$V^{(0)}_{1e,r} = -\frac{(Z - N_r)\, e^2}{r_{1e}} \tag{3.2}$$

and the term including the interaction of the perturbing electron with the internal electronic structure of the radiator along with the higher-order multipole terms has the form

$$V^{(1)}_{1e,r} = e^2 \sum_{i=1}^{N_r} \left(\frac{1}{|\boldsymbol{r}_{1e} - \boldsymbol{r}_i|} - \frac{1}{r_{1e}} \right) \tag{3.3}$$

where Z is the atomic number of the radiator, N_r is the number of bound electrons on the radiator, and x_{1e} and x_i are the positions of the perturbing electron and the i^{th} radiator electron, respectively, in the radiator's center of mass reference frame.

Under a classical treatment of the perturbing electron, the plasma electron Hamiltonian including the monopole interaction

$$H'_{1e} = K_{1e} + V^{(0)}_{1e,r} \tag{3.4}$$

describes a perturbing electron as a classical particle moving in a hyperbolic trajectory as it passes by the radiator. Under a quantum mechanical treatment of the perturbing electron, the eigenvalue problem for the plasma electron Hamiltonian is defined by

$$H'_{1e}|\, k,l,m\rangle = \frac{\hbar^2 k^2}{2m_e}|\, k,l,m\rangle \tag{3.5}$$

where $|\, k,l,m\rangle$ represents a partial wave expansion of the plasma electron state, $\hbar k$ is the momentum of the plasma electron state, and the l and m quantum numbers represent the angular momentum of this state. In the perturbing electron coordinate representation, the states $\langle \boldsymbol{x}|\, k,l,m\rangle$ are represented by Coulomb wavefunctions. The differences between the classical and quantum mechanical treatments are discussed further in the next section.

Now, let us discuss the calculation of the interaction of the perturbing electron with the internal electronic structure of the radiator. This interaction is calculated using an expansion in terms of reduced tensor operators

$$V^{(1)}_{1e,r} = e^2 \sum_{i=1}^{N_r} \sum_{t=0}^{\infty} \sum_{q=-t}^{t} A^t(r_i, r_{1e})\, C^{(t)}_q(\theta_i, \phi_i)\, C^{(t)*}_q(\theta_{1e}, \phi_{1e}) \tag{3.6}$$

where

$$A^t(r_i, r_{1e}) = \left(\frac{r_<^t}{r_>^{t+1}} - \frac{\delta_{t,0}}{r_{1e}} \right) \quad \text{and} \quad C_q^{(t)}(\theta, \phi) = \left(\frac{4\pi}{2t+1} \right)^{1/2} Y_{tq}(\theta, \phi) \,. \tag{3.7}$$

The t=0 term represents a monopole contribution between the perturbing electron and the radiator electron for perturbing electrons which penetrate the orbitals. The largest contributions to this interaction come from the $t = 0$ and the dipole ($t = 1$) terms of this expansion with relatively small contributions coming from the higher-order terms. Due to angular momentum selection rules, only a finite number of terms in this expansion give a nonzero contribution to the interaction. Even though the monopole term has been removed from this expansion, a calculation including all of the terms in the expansion is referred to throughout the remainder of this dissertation as a full-Coulomb calculation. A calculation including only the $t = 1$ term is a part of the dipole approximation, and the dipole approximation is discussed in more detail in the first section of Chapter 4.

One question that may come up at this point is why the dipole only calculation is valid in the radiator-ion interaction but not valid in the radiator-electron interaction. One must remember that for highly charged radiators, the perturbing ions experience a strong repulsion due to the monopole interaction with the radiator through the calculation of the ion microfield, and thus are not very likely to penetrate the orbitals of the radiator. Also, the terms of the expansion higher than the dipole term have been shown to have a relatively small effect [37] in comparison to the electron-broadening effects. Of course, this is definitely not the case for the perturbing electron which experiences a strong attraction to the radiator and can even penetrate the radiator orbitals, thereby resulting in significant contributions from the $t = 0$ and dipole ($t = 1$) terms.

3.2 Calculation of the Width-and-Shift Operator

As was shown in Chapter 2, the first term of the static part of the width-and-shift operator has the form

$$B^{first}(\boldsymbol{\epsilon})\boldsymbol{d}_{if} = n_e \mathrm{Tr}_{1e}\{V^{(1)}_{1e,r}\,\rho_{1e,\boldsymbol{\epsilon},r}\}\,\rho^{-1}_{\boldsymbol{\epsilon},r}\boldsymbol{d}_{if} \tag{3.8}$$

and the first term of the dynamic part of the width-and-shift operator has the form

$$M^{first}(\omega,\boldsymbol{\epsilon})\boldsymbol{d}_{if} = -\mathrm{i}n_e \int_0^\infty \mathrm{d}t\, e^{\mathrm{i}(\omega - H_{\boldsymbol{\epsilon},r} + \mathrm{i}\epsilon)t}\,\mathrm{Tr}_{1e}\Big\{\tilde{V}^{(1)}_{1e,r}(t)\,U(t,0) \cdot \rho_{1e,\boldsymbol{\epsilon},r}\,V^{(1)}_{1e,r}\,\rho^{-1}_{\boldsymbol{\epsilon},r}\,\boldsymbol{d}_{if}\,U^{\dagger}(t,0)\Big\}\,e^{\mathrm{i}H_{\boldsymbol{\epsilon},r}t}\,. \tag{3.9}$$

The time development operator has the form

$$U(t,0) = \vartheta \exp\left\{-\mathrm{i}\int_0^t \mathrm{d}t'\,\tilde{V}^{(1)}_{1e,r}(t')\right\} \tag{3.10}$$

where ϑ indicates a time-ordered calculation of the exponential term,

$$\tilde{V}^{(1)}_{1e,r}(t) = e^{\mathrm{i}(H_{\boldsymbol{\epsilon},r} + H'_{1e})t}\,V^{(1)}_{1e,r}\,e^{-\mathrm{i}(H_{\boldsymbol{\epsilon},r} + H'_{1e})t} \tag{3.11}$$

is the perturbing electron-radiator interaction in the interaction representation, and

$$H_{\boldsymbol{\epsilon},r} = H_r + \boldsymbol{d}\cdot\boldsymbol{\epsilon}\,. \tag{3.12}$$

The time development operator satisfies the differential equation

$$\mathrm{i}\hbar\frac{\partial U(t,0)}{\partial t} = \tilde{V}^{(1)}_{1e,r}(t)U(t,0)\,. \tag{3.13}$$

Note that for large t, the matrix elements of $U(t,0)$ become the S-matrix for electron scattering by the radiator [23]. In the context of this theory, these completed collisions

give the impact limit for small frequency separations near line center. For short times, $U(t,0)$ approaches 1, and an expansion of the radiator resolvent, represented by equation 2.28, in terms of the width-and-shift operator, $B_e(\epsilon) + M_e(\omega, \epsilon)$, leads to an appropriate form for the high frequency wings of the line shape [24]. The theory presented here is therefore "unified" in the sense that it describes accurately both the center and the wings of the line shape.

Continuing in this section, a classical-path approximation is applied to the trace over the perturbing electron coordinates in the width-and-shift operator. Because the perturbing electrons move in hyperbolic trajectories, a rotational transformation is also performed from an atomic collision reference frame to a hyperbolic collision reference frame in order to simplify the calculation of the matrix elements of the width-and-shift operator. We end this section by writing out the final expression for the calculation of the matrix elements of the width-and-shift operator and the matrix elements of the interaction $\tilde{V}^{(1)}_{1e,r}(t)$.

3.2.1 Classical-Path Approximation

Up to this point, the treatment of the perturbing electrons as either quantum mechanical or classical particles has not been specified. In this section, an argument is made that a classical treatment of the perturbing electrons is appropriate in the calculation of the width-and-shift operator if an appropriate length scale is applied to the problem.

In applying the classical-path approximation, the wave packets of the perturbing electrons that are not interacting with the radiator are assumed to be small enough so that they do not significantly overlap with each other [21]. Also, when the perturbing electrons interact with a highly charged radiator such as Ar^{+16} or Ar^{+17}, there is a large acceleration of the electron as it passes by the radiator, thus resulting in a smaller wave packet size in the region of the interaction. The decrease in the size of the wave packet due to the acceleration and the very short time in which the electrons remain in close

proximity to the radiator allow for a classical treatment of the perturbing electrons, even those which penetrate the orbitals of the radiator, as long as we apply a correction due to quantum diffraction effects. This correction is incorporated through a minimum distance cutoff which is discussed later in this section and also in Appendix C. One possible drawback to the smaller wave packets is that they do not hold together very long, but the electrons are also moving more quickly near the radiator and thus should hold together at least during the time of collision.

It has been previously shown that the classical-path approximation is appropriate for both the neutral and charged cases in the VCS model when [21]

$$\frac{\left|V_{1e,r}^{(1)}\right| \tau}{l\hbar} \lesssim 1 \tag{3.14}$$

where τ is the duration of the collision and $l\hbar$ is the angular momentum of the perturbing electron. This is also the condition that defines a strong collision in their model if l is on the order of one or smaller. However, this expression is appropriate only for calculations in which the monopole term due to the penetration of the orbitals is not included in the calculation.

For the case of the highly charged radiator where the monopole term due to the penetration is included, the interaction strength changes dramatically over the region of the interaction. However, this is offset by the significant acceleration of the electron near the charged radiator as the electron moves in a hyperbolic path because the electron spends less time in the region of the strongest interaction. Because the speed of the electron is affected by the charge of the radiator Z and the temperature of the electrons in the plasma $k_B T$, the largest value of the interaction $\left|V_{1e,r}^{(1)}\right|$ that we allow should be related to these quantities. The typical temperature- and Z-dependent minimum-distance cutoff applied to the minimum separation of the perturbing electron-charged

radiator collision is $r_{min} = Z\, r_{land}$, where r_{land} is the Landau length

$$r_{land} = \frac{e^2}{k_B T}. \tag{3.15}$$

This type of cutoff sets the maximum of of the electron-radiator interaction to approximately

$$\left| V^{(1)}_{1e,r} \right|_{max} \sim \frac{k_B T}{Z} \tag{3.16}$$

and assures that the strength of the interaction is balanced by the speed of the electron as it passes by the charged radiator. In Appendix C, we derive a cutoff of the form

$$r_{min} = \frac{Z\, r_{land}}{\ln g_{ij}(r \to 0)}. \tag{3.17}$$

Note that $\ln g_{ij}(r \to 0)$ modifies the cutoff for quantum diffraction effects between the perturbing electron and the radiator [40] because there is overlap between the wave packet of the perturbing electron and the radiator orbitals. With the limit on the strength of the interaction and the inclusion of quantum corrections through the cutoff, the classical-path approximation can be used for perturbing electrons interacting with highly charged radiators.

Under a classical-path approximation, there are three important changes made in the expression for the width-and-shift operator. The first change involves replacing the portion of the density matrix associated with the perturbing electron Hamiltonian with its classical analogue. This includes the treatment of the velocity distribution of the plasma electrons outside the region of interaction as being in thermal equilibrium through a Maxwell-Boltzmann distribution. This also implies that electron degeneracy effects are small, thus requiring the condition

$$E_{Fermi} \ll k_B T \tag{3.18}$$

where

$$E_{Fermi} = a_0^2 \{3\pi^2 n_e\}^{2/3} \text{ Rydbergs} \tag{3.19}$$

is the Fermi energy for a plasma of density n_e.

The second change involves the replacement of the quantum mechanical expression for the time dependent electron-radiator interaction with an expression for the interaction which depends on the classical time-dependent position and velocity of the perturbing electron in its hyperbolic trajectory about the radiator. In terms of an expression, this replacement has the form

$$\int d\boldsymbol{x} \int d\boldsymbol{x}' \, e^{i\hbar(k'^2 - k^2)t/2m_e} \langle k', l', m' | \boldsymbol{x}' \rangle \langle \boldsymbol{x}' | V^{(1)}_{1e,r}(rad) | \boldsymbol{x} \rangle \langle \boldsymbol{x} | k, l, m \rangle$$
$$\rightarrow V^{(1)}_{1e,r}(rad, x_{1e}(t), v_{1e}(t)) \tag{3.20}$$

where "rad" indicates the dependence on the internal states of the radiator and $|k, l, m\rangle$ represents a partial wave expansion of the perturbing-electron state. As stated in the previous section, these states are the appropriate eigenfunctions for the electron Hamiltonian H'_{1e}

$$H'_{1e} | k, l, m \rangle = \frac{\hbar^2 k^2}{2m_e} | k, l, m \rangle \,, \tag{3.21}$$

and in the perturbing electron coordinate representation, the states $\langle \boldsymbol{x} | k, l, m \rangle$ are represented by Coulomb wavefunctions.

The third change involves the calculation of the one-electron trace over the free electron perturber states. In the quantum mechanical calculation, the one-electron trace is written as an integral over momenta states and a sum over angular momenta states

$$\text{Tr}_{1e}\{\cdots\} = \sum_{l=0}^{\infty} \sum_{m=-l}^{l} \int_0^{k_{Deb}} dk \, k^2 \langle k, m, l | \cdots | k, l, m \rangle \,. \tag{3.22}$$

Under the classical-path approximation, the one-electron trace for the electron trajectory has the form

$$\mathrm{Tr}_{1e}\{\cdots\} = \int_0^\infty \mathrm{d}v_\infty \, 4\pi \int_{b_{min}}^{b_{Deb}} \mathrm{d}b \, 2\pi b \int_0^{t_{col}} \mathrm{d}t_0 \, v_\infty \int \frac{\mathrm{d}\Omega}{8\pi^2} \{\cdots\} \tag{3.23}$$

The variables v_∞ (speed outside interaction region), b (impact parameter), and Ω (orientation of trajectory) define an unique hyperbolic path about the radiator. The lower cutoff on the impact parameter is set so that the minimum distance of approach between the electron and the radiator is given by Equation 3.17. In order to account for the removal of electron correlations, the upper limit on the impact parameter is set so that electrons outside a sphere of radius the Debye length are effectively screened from the radiator. In order to define the initial position of the electron on the hyperbola, we also need to integrate over the time t_0 that it takes the electron to leave the interaction region while moving from any point within this region along its hyperbolic trajectory. In other words, we sum up the contributions from all possible incomplete collisions. The upper limit t_{col} is the total time that it takes an electron to move through the interaction region along its trajectory. Note that during the time $\mathrm{d}t_0$, the number of electrons that begin a collision with the radiator is given by $n_\epsilon(2\pi b \, \mathrm{d}b)v_\infty \, \mathrm{d}t_0$. Also, the integration over this electron number, multiplied by the velocity distribution of the plasma electrons outside the interaction region, gives the appropriate average over all possible collisions of the free electrons with the radiator for a given orientation of the electron trajectories.

Throughout the rest of this work, the classical description of the perturbing electrons is used, including the classical forms of the electron-radiator interaction and the one-electron trace.

3.2.2 Radiator Basis and the Matrix Elements of $M'(\omega, \epsilon)$

A complete set of basis states must now be chosen for the isolated radiator in order to calculate the matrix elements of the width-and-shift operator. Because the radiator

species considered in this dissertation must be treated relativistically, the natural energy basis for the isolated radiator is the total angular momentum energy basis $|\alpha, j, m\rangle$, where α represents all of the quantum numbers excluding j and m. Primes on the quantum numbers refer to a lower or final state of the transition.

Because the classical trajectories of the perturbing electrons in the charged-radiator problem are hyperbolic, it is useful to perform a rotational transformation from an atomic collision reference frame in which the microfield ϵ points along the z-axis to a hyperbolic collision reference frame when calculating the matrix elements of the width-and-shift operator. In the hyperbolic frame, the x-axis is aligned so that it points outward from the radiator toward the point of closest approach of the perturbing electron in its hyperbolic trajectory. The z-axis points outward from the radiator perpendicular to the plane of the trajectory. The time development operator in this hyperbolic frame is given by [25]

$$U_h(t,0) = D(\Omega)U(t,0)D^{-1}(\Omega) \tag{3.24}$$

where $D(\Omega)$ is the rotation operator which rotates from the atomic collision frame mentioned above to the hyperbolic collision frame. This time development operator satisfies the differential equation

$$i\hbar\frac{\partial U_h(t,0)}{\partial t} = \tilde{V}_h(t)U_h(t,0) \tag{3.25}$$

where

$$\tilde{V}_h(t) = D(\Omega)\tilde{V}^{(1)}_{1e,r}(t)D^{-1}(\Omega) \tag{3.26}$$

is the electron-radiator interaction as seen in the hyperbolic frame.

Using the total angular momentum basis set and the rotational transformation mentioned above, the matrix elements of the static part of the width-and-shift operator have

the form

$$\langle \alpha_a^{'}, j_a^{'}, m_a^{'}; \alpha_a, j_a, m_a \,|\, B^{first}(\boldsymbol{\epsilon}) |\, \alpha_b^{'}, j_b^{'}, m_b^{'}; \alpha_b, j_b, m_b \rangle = n_e \int_0^\infty \mathrm{d}v_\infty \, 4\pi$$
$$\times \int_{b_{min}}^{b_{Deb}} \mathrm{d}b \, 2\pi b \int_0^{t_{col}} \mathrm{d}t_0 \, v_\infty \int \frac{\mathrm{d}\Omega}{8\pi^2} \sum_{m_c, m_d} \Big\{ D^{(j_a)-1}_{m_a, m_c} \langle \alpha_a, j_a, m_c \,|$$
$$\times V_h(0) \, \rho^{(h)}_{1\epsilon, \epsilon, r} \, \rho^{(h)-1}_{\epsilon, r} \,|\, \alpha_b, j_b, m_d \rangle D^{(j_b)}_{m_d, m_b} \Big\} \delta_{\alpha_a^{'}, \alpha_b} \delta_{j_a^{'}, j_b^{'}} \delta_{m_a^{'}, m_b^{'}} \tag{3.27}$$

and the matrix elements of the dynamic part of the width-and-shift operator have the form

$$\langle \alpha_a^{'}, j_a^{'}, m_a^{'}; \alpha_a, j_a, m_a \,|\, M^{first}(\omega, \boldsymbol{\epsilon}) |\, \alpha_b^{'}, j_b^{'}, m_b^{'}; \alpha_b, j_b, m_b \rangle = -\mathrm{i} n_e \int_0^\infty \mathrm{d}t$$
$$\times e^{\mathrm{i}(\omega + \mathrm{i}\varepsilon)t} \int_0^\infty \mathrm{d}v_\infty \, 4\pi \int_{b_{min}}^{b_{Deb}} \mathrm{d}b \, 2\pi b \int_0^{t_{col}} \mathrm{d}t_0 \, v_\infty \int \frac{\mathrm{d}\Omega}{8\pi^2} \sum_{m_c, m_d, m_c^{'}, m_d^{'}} \Big\{ D^{(j_a)-1}_{m_a, m_c}$$
$$\times \langle \alpha_a, j_a, m_c \,|\, e^{-\mathrm{i}H^{(h)}_{\epsilon, r} t/\hbar} \bar{V}_h(t) \, U_h(t, 0) \, \rho^{(h)}_{1\epsilon, \epsilon, r} \, V_h(0) \, \rho^{(h)-1}_{\epsilon, r} \,|\, \alpha_b, j_b, m_d \rangle$$
$$\times D^{(j_b)}_{m_d, m_b} D^{(j_b^{'})-1}_{m_b^{'}, m_d^{'}} \langle \alpha_b^{'}, j_b^{'}, m_d^{'} \,|U_h^\dagger(t, 0) \, e^{\mathrm{i}H^{(h)}_{\epsilon, r} t}|\, \alpha_a^{'}, j_a^{'}, m_c^{'} \rangle D^{(j_a^{'})}_{m_c^{'}, m_a^{'}} \Big\} \tag{3.28}$$

where

$$\rho^{(h)}_{\epsilon, r} = D(\Omega) \rho_{\epsilon, r} D(\Omega)^{-1} \tag{3.29}$$

$$\rho^{(h)}_{1\epsilon, \epsilon, r} = D(\Omega) \rho_{1\epsilon, \epsilon, r} D(\Omega)^{-1} \tag{3.30}$$

$$H^{(h)}_{\epsilon, r} = H_r + D(\Omega)(\boldsymbol{d} \cdot \boldsymbol{\epsilon}) D(\Omega)^{-1} \tag{3.31}$$

and

$$D^{(j)}_{m, m'} = \langle n, j, m |\, D(\Omega) |n, j, m' \rangle \,. \tag{3.32}$$

The only terms in the calculation of the matrix elements of the static and dynamic width-and-shift operator which are dependent on the orientation of the trajectory Ω are the Stark-broadening terms $\boldsymbol{d} \cdot \boldsymbol{\epsilon}$ and the matrix elements of the rotation operators $D^{(j)}_{m, m'}$. All other terms are spherically symmetric.

To simplify this expression further, an approximation is needed to deal with the Ω dependence of the Stark-broadening term. At this point, we remove the dependence of the width-and-shift operator on the ion microfield ϵ, as was done in other models [18], thereby leaving the rotation terms $D^{(j)}_{m\,,m'}$ outside of both the time development operator and the reduced distribution functions as the only terms dependent on Ω. With this approximation, the expressions

$$\langle\,\Omega\rangle_{\,1} \equiv \int \frac{\mathrm{d}\Omega}{8\pi^2}\, D^{(j_a)\,-1}_{m_a,m_c}\, D^{(j_b)}_{m_d,m_b} \tag{3.33}$$

$$\langle\Omega\rangle_{\,2} \equiv \int \frac{\mathrm{d}\Omega}{8\pi^2}\, D^{(j_a)\,-1}_{m_a,m_c}\, D^{(j_b)}_{m_d,m_b}\, D^{(j_b')\,-1}_{m_b',m_d'}\, D^{(j_a')}_{m_c',m_a'} \tag{3.34}$$

represent a spherical average over all possible orientations of the electron trajectories. The calculational details of these averages have been presented in previous papers by various authors [24,25]. Thus, the matrix elements of the width-and-shift operator under these averages have the form

$$\begin{aligned}\langle\,\alpha_a^{'}\,,j_a^{'}\,,m_a^{'}\,;\alpha_a\,,j_a\,,m_a\,|\,B^{first}|\,\alpha_b^{'}\,,j_b^{'}\,,m_b^{'}\,;\alpha_b\,,j_b\,,m_b\,\rangle &= n_e \int_0^\infty \mathrm{d}v_\infty\, 4\pi \\ \times \int_{b_{min}}^{b_{Deb}} \mathrm{d}b\, 2\pi b \int_0^{t_{col}} \mathrm{d}t_0\, v_\infty \frac{1}{2j_a+1} \sum_{m_c} &\left\{\langle\,\alpha_a\,,j_a\,,m_c\,|\,V_h(0)\,\rho_{1e,r}\,\rho_r^{-1}\right. \\ \left.\times\,|\,\alpha_b\,,j_a\,,m_c\,\rangle\right\} &\delta_{j_a,j_b}\delta_{m_a,m_b}\delta_{\alpha_a',\alpha_b'}\delta_{j_a',j_b'}\delta_{m_a',m_b'}\end{aligned} \tag{3.35}$$

and

$$\begin{aligned}\langle\,\alpha_a^{'}\,,j_a^{'}\,,m_a^{'}\,;\alpha_a\,,j_a\,,m_a\,|\,M^{first}(\omega)|\,\alpha_b^{'}\,,j_b^{'}\,,m_b^{'}\,;\alpha_b\,,j_b\,,m_b\,\rangle &= -\mathrm{i}n_e \int_0^\infty \mathrm{d}t \\ \times\, e^{\mathrm{i}(\omega+\mathrm{i}\epsilon)t} \int_0^\infty \mathrm{d}v_\infty\, 4\pi \int_{b_{min}}^{b_{Deb}} \mathrm{d}b\, 2\pi b \int_0^{t_{col}} \mathrm{d}t_0\, v_\infty \sum_{m_c,m_d,m_c',m_d'} &\langle\,\Omega\rangle_{\,2} \\ \times \Big\{\langle\,\alpha_a\,,j_a\,,m_c\,|e^{-\mathrm{i}H_r t/\hbar}\,\tilde{V}_h(t)\,U_h(t,0)\,\rho_{1e,r}\,V_h(0)\,\rho_r^{-1}|\,\alpha_b\,,j_b\,,m_d\,\rangle &\\ \times\,\langle\,\alpha_b^{'}\,,j_b^{'}\,,m_d^{'}|U_h^{\dagger}(t,0)e^{\mathrm{i}H_r t/\hbar}|\,\alpha_a^{'}\,,j_a^{'}\,,m_c^{'}\rangle\Big\}. &\end{aligned} \tag{3.36}$$

If final-state broadening effects are to be left out of the calculation, the first term of the dynamic part of the width-and-shift operator must be modified to maintain consistency by replacing $U^{\dagger}(t,0)$ with the unity operator. Therefore,

$$\sum_{m_c,m_d,m_c',m_d'} \langle\Omega\rangle_2 \{\cdots\} \rightarrow \sum_{m_c,m_d} \langle\Omega\rangle_1 \{\cdots\}, \tag{3.37}$$

and the dynamic part simplifies in a manner similar to that of the static part. The first term of the static part does not contain any final-state broadening contributions and remains unchanged. Therefore, the matrix elements of the static and dynamic parts of the width-and-shift operator are now given by

$$\begin{aligned}\langle \alpha_a', j_a', m_a'; \alpha_a, j_a, m_a | B^{initial} | \alpha_b', j_b', m_b'; \alpha_b, j_b, m_b \rangle &= n_e \int_0^{\infty} \mathrm{d}v_{\infty} 4\pi \\ \times \int_{b_{min}}^{b_{Deb}} \mathrm{d}b\, 2\pi b \int_0^{t_{col}} \mathrm{d}t_0\, v_{\infty} \frac{1}{2j_a+1} \sum_{m_c} \{ &\langle \alpha_a, j_a, m_c | V_h(0) \rho_{1e,r} \rho_r^{-1} \\ \times | \alpha_b, j_a, m_c \rangle \} \delta_{j_a,j_b} \delta_{m_a,m_b} &\delta_{\alpha_a',\alpha_b'} \delta_{j_a',j_b'} \delta_{m_a',m_b'}\end{aligned} \tag{3.38}$$

and

$$\begin{aligned}\langle \alpha_a', j_a', m_a'; \alpha_a, j_a, m_a | M^{first}(\omega) | \alpha_b', j_b', m_b'; \alpha_b, j_b, m_b \rangle &= -\mathrm{i}n_e \int_0^{\infty} \mathrm{d}t \\ \times e^{\mathrm{i}(\omega+\mathrm{i}\epsilon)t} \int_0^{\infty} \mathrm{d}v_{\infty} 4\pi \int_{b_{min}}^{b_{Deb}} \mathrm{d}b\, 2\pi b \int_0^{t_{col}} \mathrm{d}t_0\, v_{\infty} \frac{1}{2j_a+1} \sum_{m_c} \{ &\langle \alpha_a, j_a, m_c | \\ \times e^{-\mathrm{i}H_r t/\hbar} \tilde{V}_h(t)\, U_h(t,0)\, \rho_{1e,r}\, V_h(0)\, \rho_r^{-1} | \alpha_b, j_a, m_c \rangle &\langle \alpha_a', j_a', m_a' | e^{\mathrm{i}H_r t/\hbar} \\ \times | \alpha_a', j_a', m_a' \rangle \Big\} \delta_{j_a,j_b} \delta_{m_a,m_b} &\delta_{\alpha_a',\alpha_b'} \delta_{j_a',j_b'} \delta_{m_a',m_b'}.\end{aligned} \tag{3.39}$$

To calculate the matrix elements of the width-and-shift operator for initial-state broadening, matrix elements of the time development operator and of the electron-radiator interaction $V_h(t)$ over the initial states are needed. To preserve the appropriate time ordering of the interaction terms in the expansion of the time development operator,

a coupled set of first-order differential equations of the form

$$i\hbar\frac{\partial}{\partial t}\langle \alpha_a, j_a, m_a|U_h(t,0)|\alpha_b, j_b, m_b\rangle = \sum_{\alpha_c, j_c, m_c}\langle \alpha_a, j_a, m_a|V_h(t) \times|\alpha_c, j_c, m_c\rangle\langle \alpha_c, j_c, m_c|U_h(t,0)|\alpha_b, j_b, m_b\rangle \tag{3.40}$$

must be solved. The number of differential equations in this coupled set is N^2, where N is the number of radiator states included in the initial-state manifold. Many of these matrix elements are zero because of angular momentum selection rules in the calculation of the matrix elements of $V_h(t)$.

As a matter of convenience, another reference frame can be defined in which the x-axis moves with the electron as it traverses its hyperbolic trajectory past the radiator. The rotation operator that defines the rotation from the hyperbolic reference frame to this rotating reference frame is be given by

$$D(\phi_{1e}(t)) = e^{-i\phi_{1e}(t)J_z/\hbar} \tag{3.41}$$

where $\phi_{1e}(t)$ is the azimuthal angle and J_z is the z^{th} component of the total angular momentum operator. With this rotation, the matrix elements of the electron-radiator interaction in the hyperbolic frame can be written in the form

$$\langle \alpha_a, j_a, m_a|V_h(t)|\alpha_b, j_b, m_b\rangle = e^{i(m_a-m_b)\phi_{1e}(t)} \times\langle \alpha_a, j_a, m_a|V_{rot}(t)|\alpha_b, j_b, m_b\rangle \tag{3.42}$$

where $V_{rot}(t)$ is the electron-radiator interaction in this rotating reference frame. Keeping in mind that the electron coordinates are being treated classically, the radiator matrix

elements of this interaction can be given by

$$\langle \alpha_a, j_a, m_a | V_{rot}(t) | \alpha_b, j_b, m_b \rangle = (-1)^{j_a - m_a} \sum_{t=0}^{\infty} \sum_{q=-t}^{t} \times \langle \alpha_a, j_a || \sum_{i=1}^{N_r} A_i^t(r_{1e}) C_i^{(t)} || \alpha_b, j_b \rangle C_q^{t*} \left(\frac{\pi}{2}, 0 \right) \begin{pmatrix} j_a & t & j_b \\ -m_a & q & m_b \end{pmatrix} \quad (3.43)$$

with the application of the Wigner-Eckart theorem [41,42]. Note that in this rotating reference frame, $\theta_{1e}(t) = \pi/2$ and $\phi_{1e}(t) = 0$.

The reason for writing the potential in terms of irreducible tensor operators and then applying the Wigner-Eckart theorem is now clear. The selection rules for the occurrence of nonzero matrix elements of the interaction are now embodied in the calculation of the 3J symbol

$$\begin{pmatrix} j_a & t & j_b \\ -m_a & q & m_b \end{pmatrix} \quad (3.44)$$

which is zero unless the triangle relations

$$t \geqq |j_a - j_b| \quad (3.45)$$

$$t \leqq j_a + j_b \quad (3.46)$$

$$t \geqq |q| \quad (3.47)$$

$$q = m_a - m_b \quad (3.48)$$

hold. Further properties of the 3J symbols are discussed in Appendix D. Therefore,

$$\langle \alpha_a, j_a, m_a | V_{rot}(t) | \alpha_b, j_b, m_b \rangle = (-1)^{j_a - m_a} \sum_{t=max[|m_a - m_b|,|j_a - j_b|]}^{j_a + j_b} \times \langle \alpha_a, j_a || \sum_{i=1}^{N_r} A_i^t(r_{1e}) C_i^{(t)} || \alpha_b, j_b \rangle C^t_{m_a - m_b}{}^* \left(\frac{\pi}{2}, 0\right) \times \begin{pmatrix} j_a & t & j_b \\ -m_a & m_a - m_b & m_b \end{pmatrix}. \tag{3.49}$$

The line shapes to be presented in this dissertation result from transitions in hydrogenic radiators. Therefore, the next step is to uncouple the spin angular momenta from the orbital angular momenta. Because the interaction $V_{rot}(t)$ does not depend on the spin coordinates, the matrix elements of this interaction have the form

$$\langle \alpha_a, j_a, m_a | V_{rot}(t) | \alpha_b, j_b, m_b \rangle = \delta_{s_a, s_b} (-1)^{j_a - m_a + j_b + s_a} ([j_a, j_b][l_a, l_b])^{1/2} \times \sum_{t=\max[|m_a - m_b|,|j_a - j_b|,|l_a - l_b|]}^{\min[j_a + j_b, l_a + l_b]} \langle n_a, l_a || A^t(r_{1e}) || n_b, l_b \rangle C^t_{m_a - m_b}{}^* \left(\frac{\pi}{2}, 0\right) \times \begin{pmatrix} l_a & t & l_b \\ 0 & 0 & 0 \end{pmatrix} \begin{pmatrix} j_a & t & j_b \\ -m_a & m_a - m_b & m_b \end{pmatrix} (-1)^t \begin{Bmatrix} l_a & s_a & j_a \\ j_b & t & l_b \end{Bmatrix} \tag{3.50}$$

where the last term is a 6J symbol and the definitions

$$[l_a, l_b, \cdots] \equiv (2l_a + 1)(2l_b + 1) \cdots \tag{3.51}$$

$$\langle n_a, l_a || A^t(r_{1e}) C_i^{(t)} || n_b, l_b \rangle \equiv (-1)^{l_a} [l_a, l_b]^{1/2} \begin{pmatrix} l_a & t & l_b \\ 0 & 0 & 0 \end{pmatrix} \times \langle n_a, l_a || A^t(r_{1e}) || n_b, l_b \rangle \tag{3.52}$$

have been used. The definition of the 6J symbol is given in Appendix D, along with the specific treatment of the 6J symbol occurring in this expression. Also, note that the uncoupling of the orbital and spin angular momenta places a third constraint on the summation over t. Finally, the reduced matrix element in the t^{th} term of the multipole expansion is given by

$$\langle n_a, l_a || A^t(r_{1e}) || n_b, l_b \rangle = \int_0^\infty \mathrm{d}r\, r^2\, R^*_{n_a,l_a}(r) \left(\frac{r_<^t}{r_>^{t+1}} - \frac{\delta_{t,0}}{r_{1e}} \right) R_{n_b,l_b}(r) \qquad (3.53)$$

where $R_{n_b,l_b}(r)$ are the relativistic radial wave functions.

In the next chapter, we begin by discussing the computational methods used in calculating the width-and-shift operator described in the current chapter and its incorporation into the calculation of theoretical spectral lines. We then discuss the various effects of the width-and-shift operator on the shape and location of the theoretical spectral lines. Comparisons are then made between calculated spectral lines utilizing the electron-broadening model described in this chapter and calculated spectral lines utilizing other electron-broadening models. The process of line merging is also discussed.

CHAPTER 4
COMPUTATIONAL ANALYSIS

In this chapter, the computational methods and results of the semiclassical (classical-path) model to all-order in the full-Coulomb electron-radiator interaction as described in the previous chapters are discussed in detail. The dependencies of line widths and shifts on various plasma and radiator state parameters are considered. Comparisons of calculated line shapes using full-Coulomb and dipole-approximation versions of the semiclassical all-order model are shown to demonstrate the importance of the full-Coulomb treatment of the electron-radiator interaction. We then compare calculated lines shapes using full-Coulomb and dipole-approximation versions of both the semiclassical all-order model and the quantum mechanical model to second-order in the electron-radiator interaction. We show that the full-Coulomb all-order and second-order models in the electron-radiator interaction differ mainly in the wings of the line shape and in the calculation of merging lines. Note that all line shapes shown throughout this chapter are calculated with an atomic fraction concentration of 1% Argon in D_2 because the width-and-shift operator does not depend on this concentration.

4.1 Computational Methods

The computation of spectra has been broken into two parts. The first part involves the calculation of matrix elements of a width-and-shift operator using a code based on the expressions presented in the previous chapter. The width-and-shift values are incorporated into a second code which uses these values to generate theoretical spectra. The theoretical spectra can then be used to analyze experimental spectral data. This section concentrates on the computation of line widths and shifts and the corresponding theoretical spectra.

To calculate the line widths and shifts and the line profiles, information concerning the the relativistic atomic physics must first be incorporated into the computational codes. The line shape code and the width-and-shift code written by the author of this dissertation require as input the relativistic energy level structure generated by a suite of atomic physics codes written by Robert Cowan at Los Alamos National Laboratory [43]. In addition, relativistic radial wavefunctions for the bound-electron states are extracted from this suite of atomic physics codes to be used in the width-and-shift code.

The calculation of the width-and-shift values begins with the generation of the matrix elements of the full-Coulomb electron-radiator interaction in the rotating reference frame $\langle \alpha_a , j_a , m_a | V_{rot}(t) | \alpha_b , j_b , m_b \rangle$ as described in the previous chapter. The advantage of using this rotating reference frame is that the matrix elements are not dependent on the azimuthal angle $\phi(t)$ and are only dependent on the perturbing electron's radial distance from the center of the radiator, thereby reducing the memory needed for storage. Remember that in this rotating reference frame, the z-axis is perpendicular to the plane of the trajectory, and the x-axis moves with the perturbing electron as it traverses its hyperbolic trajectory. The purpose of calculating the matrix elements first and then storing them in memory is that it is much faster to read them from memory then it is to generate them as they are needed in the calculation of the width-and-shift values.

To calculate these matrix elements, the reduced matrix elements of the irreducible radial tensor operator $\langle n_a , l_a || A^t(r_{1e}) || n_b , l_b \rangle$ are needed, and these require the relativistic radial wavefunctions $R_{n,l}(r)$. Although the radial wavefunctions for the hydrogenic radiator problem can be generated easily, the radial wavefunctions used in this model are extracted from Cowan's suite of atomic physics codes. This approach allows for an easier expansion of this code to handle helium-like radiators where the calculation of the relativistic radial wavefunctions are no longer quite as simple.

After the calculation of the matrix elements of the electron-radiator interaction, the integrations over the initial electron velocity v_∞, the impact parameter b, and the time

of closest approach t_0 are carried out over the appropriate limits on the integrands of both the static B and dynamic $M(\omega)$ parts of the width-and-shift operator. In addition to the dependence of these integrands on the matrix elements of the electron-radiator interaction, the integrand of the dynamic part also depends on matrix elements of the time development operator. The placement and calculation of the integrand points are weighted more heavily in those regions in which the integrand is changing most rapidly. These three integrations represent the one-electron trace as defined in the previous chapter.

For each value of the initial electron velocity and the impact parameter, the matrix elements of the time development operator need to be calculated. This is accomplished by solving a coupled set of first-order differential equations of the matrix elements of the time development operator, thereby including the appropriate time ordering in the time development operator. These differential equations depend specifically on the behavior of the matrix elements of the electron-radiator interaction. Out of the different ordinary differential equation solvers that were tested, a 4^{th} order Runge-Kutta solver adjusted for complex numbers with 5^{th} order error checking resulted in the most efficient calculation of this set of first-order differential equations.

The final step in the calculation of the width-and-shift values is to calculate the Laplace transform in the dynamic part of the width-and-shift operator. This transform is relatively simple to calculate. Most of the calculational effort in obtaining the width-and-shift values occurs in the calculation of the one-electron trace in the dynamic part of the width-and-shift operator due to its dependence on the time development operator. The dynamic part generally takes about 100 times longer than the static part to calculate.

To generate the theoretical spectra, a previous line shape code known as MERL [35,44] is used with the exception that the quantum mechanical, multi-electron, dipole-approximation treatment of the electron width-and-shift operator is replaced with the model presented in this dissertation. In order to function, this line shape code needs

the energy level structure of the radiator. It also needs the reduced dipole matrix elements that are used in the calculation of the radiator dipole autocorrelation function and the Stark splitting term. As stated above, this information is supplied by Cowan's suite of atomic physics codes.

If one wishes to calculate the width-and-shift values under the dipole approximation, the same procedure stated above for calculating the width-and-shift operator can be used with two exceptions. The first exception is to keep only the dipole term in the multipole expansion of the electron-radiator interaction $V^{(1)}_{1e,r}$. The monopole contribution $V^{(0)}_{1e,r}$ that was added to the perturbing electron Hamiltonian is not affected by this approximation. The second exception is to set the lower limit on the integration over the impact parameter to zero to compensate for ignoring the monopole orbital penetration term. Because almost all of the static shift results from this monopole term, there is no significant shift and distortion under the dipole approximation. This classical version of the dipole approximation is analogous to the quantum mechanical dipole approximation used in MERL.

4.2 Analysis of Line Widths and Shifts

In this section, line spectra calculated from a semiclassical model to all-order in the perturbing electron-radiator interaction (SC all-order model) is presented with a focus on spectra from hydrogenic argon radiators, Ar^{+17}, immersed in the plasma. Dependencies of the width-and-shift of line shapes on the electron density and temperature and on the principal and orbital angular momentum quantum numbers is discussed in some detail.

In general, the width and shift of spectral lines increases with increasing principal quantum number n of the upper states of a transition in a Rydberg series. The physical reasoning for this behavior is that the higher-lying energy shells of the radiator provide a larger spatial volume for the interaction of the perturbing electron with the corresponding radiator state, or in other words, the higher n states are less tightly bound

and more easily perturbed. Also, the sub-shells with lower orbital angular momentum l provide a larger spatial volume for the interaction. Thus, the spherical $l = 0$ or s orbital experiences the largest width and shift, with smaller width-and-shift values as l increases. This behavior is shown in Figure 4.1 for width-and-shift values at line center with an electron density of 1×10^{24} cm^{-3} over a range of temperatures.

From the expression for the width-and-shift operator in Chapter 3, it is clear that this operator is nearly linear in the electron density n_e. The Debye screening cutoff introduces a slight deviation from this linear dependence. Thus, the width and shift increases with increasing electron density. The physical reasoning for this behavior is that as the electron density increases, a larger number of binary collisions occur between the radiator and perturbing electrons during the lifetime of the upper state of the transition, thereby resulting in larger electron-broadening effects. This behavior is shown in Figure 4.2 using a full-Coulomb treatment of the perturbing electron-radiator interaction and in Figure 4.3 using a dipole approximation to this interaction. Therefore, we have shown, as was stated at the end of Section 4.1, that the line profiles in the full-Coulomb calculation experience a significant amount of shift and distortion while the line profiles in the dipole-approximation calculation experience very little shift and are relatively symmetric. When the density becomes sufficiently high, the shift and possibly the distortion in the line profile should be noticeable in the experimental data, and thus a dipole-approximation calculation is no longer adequate.

The large shift in the full-Coulomb calculation of the spectral lines, in addition to being a useful density diagnostic, gives rise to some very interesting physics. Because a higher-lying spectral line in a Rydberg series shifts by a larger amount than the adjacent lower spectral line of the series, they can begin to merge together when the density becomes large enough. Further details on the process of line merging are given in the next section.

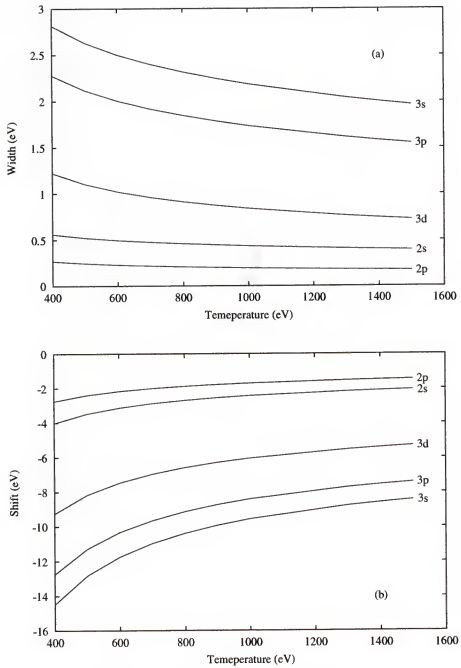

Figure 4.1: This figure shows level widths and shifts due to electron broadening for the Ar^{+17} Lyman series as a function of temperature at an electron density of 1×10^{24} cm^{-3}. Note that the values of the widths and shifts increase with principal quantum number and decrease with increasing orbital angular momentum quantum number. a) The widths are shown. b) The shifts are shown.

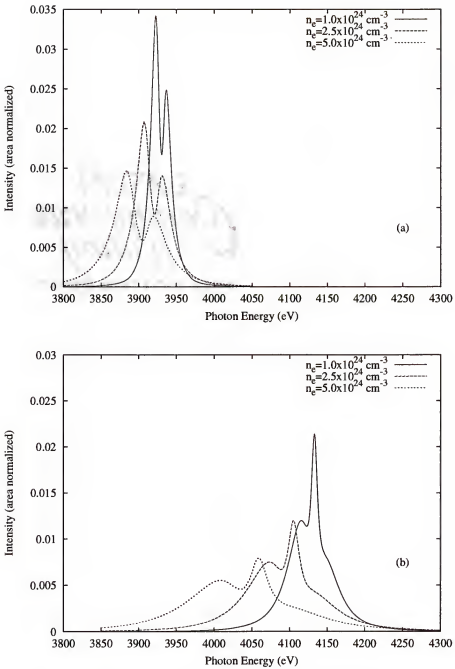

Figure 4.2: Line shapes of hydrogen-like argon utilizing a full-Coulomb calculation of the electron-radiator interaction are shown as a function of electron density with a temperature of $k_B T = 1$ keV. The width and shift of the line shapes increases as density increases. Also, note that the line shapes contain a distortion due to the differing shifts of the levels. a) The Ar^{+17} Ly-β line is shown. b) The Ar^{+17} Ly-γ line is shown.

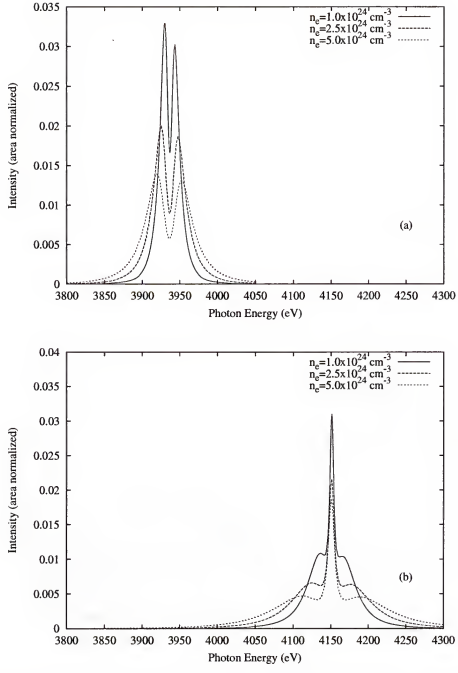

Figure 4.3: Line shapes of hydrogen-like argon calculated in the dipole approximation of the electron-radiator interaction are shown as a function of electron density with a temperature of $k_B T = 1$ keV. Note that there are no shifts and small asymmetries in the line shapes under the dipole approximation. a) The Ar^{+17} Ly-β line is shown; b) The Ar^{+17} Ly-γ line is shown.

Although strongly dependent on the electron density, it can be seen from Figure 4.1 that the width-and-shift values due to electron broadening are relatively weakly dependent on the electron temperature. This figure shows that as the temperature of the electrons increases, the width-and-shift values decrease. The physical reasoning for this is relatively simple. As the plasma electrons increase in temperature, the average speed of the electrons in the plasma also increases. Therefore, as the electrons speed past the radiator in their hyperbolic trajectory, there is less time for them to interact with the radiator thus resulting in smaller perturbation effects on the orbitals of the radiator.

What is the effect of this temperature dependence on the line spectra? The answer to this question depends on whether a full-Coulomb or a dipole-approximation treatment is applied to the perturbing electron-radiator interaction in the calculation of the width and shift. As can be seen in Figure 4.4, line spectra utilizing a dipole approximation change by small amounts with changes in temperature. However, as can be seen in Figure 4.5, line asymmetries in the theoretical spectra utilizing a full-Coulomb treatment of the electron-radiator interaction become more pronounced as the plasma electron temperature decreases.

These asymmetries arise because of a significant amount of differing shifts in the angular momentum states of the radiator due to the penetrating monopole contribution, as can be observed in Figure 4.1. The theoretical $\beta-$ and γ-lines in Figure 4.5 represent $3p - 1s$ and $4p - 1s$ transitions, respectively. Due to the ion Stark splitting of the line, the upper level p states are mixed with other angular momentum states, thus giving rise to differential shifting of the Stark components. This, in turn, gives rise to the asymmetries seen in the line shape.

4.3 Comparison with Other Models

In this section, comparisons are made between the results of the SC all-order model and a quantum mechanical model to second-order in the radiator-perturbing

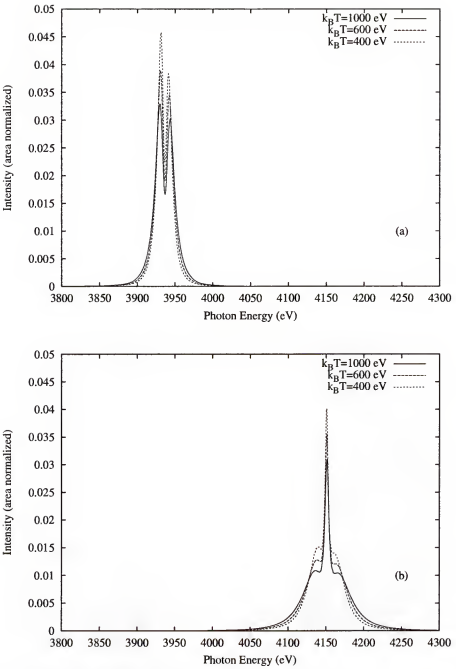

Figure 4.4: Line shapes of hydrogen-like argon calculated in the dipole approximation of the electron-radiator interaction are shown as a function of temperature with a with a density of $n_e = 1 \times 10^{24}$ cm^{-3}. There are no shifts and small asymmetries in the line shapes, and the temperature dependence is not as pronounced as is seen in Figure 4.5. a) The Ar^{+17} Ly-β line is shown; b) The Ar^{+17} Ly-γ line is shown.

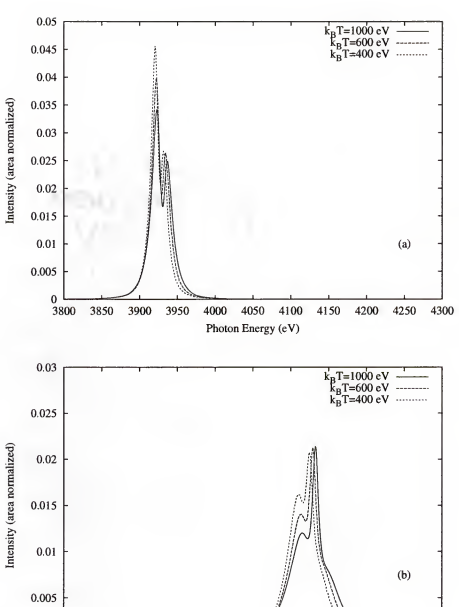

Figure 4.5: Line shapes of hydrogen-like argon utilizing a full-Coulomb calculation of the electron-radiator interaction are shown as a function of temperature with a density of $n_e = 1 \times 10^{24}$ cm^{-3}. The differing shifts of the levels cause increasing asymmetry as the temperature decreases. a) The Ar^{+17} Ly-β line is shown. b) The Ar^{+17} Ly-γ line is shown.

electron interaction (QM second-order model) using both a full-Coulomb and a dipole-approximation treatment of this interaction. Through comparisons of the results of the two models, we demonstrate the plasma conditions under which the second-order model begins to break down, specifically in the calculation of the far wings of the line shape and calculations of adjacent spectral lines in a Rydberg series that begin to overlap.

We begin by first showing the comparisons in Figure 4.6 of the theoretical Lyman-β and Lyman-γ line profiles from both QM second-order and SC all-order models using a dipole-approximation calculation at a typical ICF electron density and temperature of 1×10^{24} cm^{-3} and 1 keV, respectively. We can see that the QM second-order model gives a line profile which is noticeably more broad than our SC all-order model. It has also been shown that in these QM second-order models, a dipole-approximation calculation generally overestimates the width of a line [18]. As can be seen in Figures 4.2 and 4.3, there does not seem to be quite as large a discrepancy in the SC all-order model. In fact, the comparisons of line shapes between versions of the SC all-order model using dipole-approximation and full-Coulomb treatments of the electron-radiator interaction show that the dipole-approximation line shapes are somewhat more narrow than the full-Coulomb line shapes. In Figure 4.7, we also show comparisons of full-Coulomb theoretical Lyman-β and Lyman-γ line profiles from both the SC all-order and the QM second-order models at the same density and temperature stated above. We see that these two line profiles are in good agreement having basically the same width and shift.

As plasmas become more strongly coupled, as is the case when the temperature decreases or the density increases, the validity of a second-order theory comes into question. If we keep the temperature at 1 keV and raise the electron density to 5×10^{24} cm^{-3}, the comparison of the full-Coulomb SC all-order and QM second-order models in Figure 4.8 still show good agreement for the isolated line shape calculation. However, this does not hold true when mixing is included between the upper-state manifolds of adjacent lines, as is demonstrated at the end of this section. If we instead keep

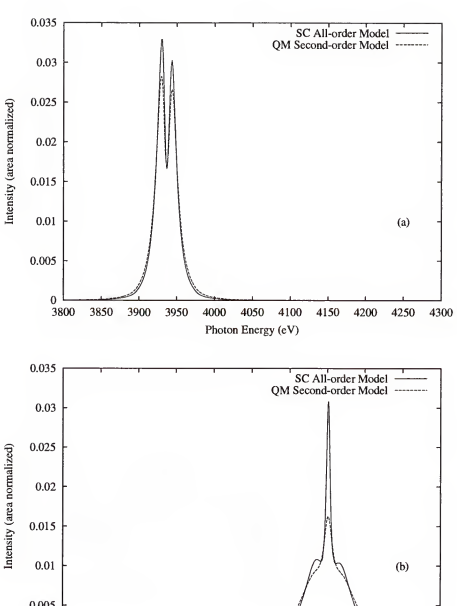

Figure 4.6: This figure shows comparisons of hydrogen-like argon spectra from the dipole-approximation version of the SC all-order and QM second-order models at an electron density and temperature of 1×10^{24} cm^{-3} and 1 keV, respectively. Note that in the dipole approximation, the QM second-order model calculates line shapes which are broader than those from the SC all-order model. a) This plot shows the Lyman-β line of Ar^{+17}. b) This plot shows the Lyman-γ line of Ar^{+17}.

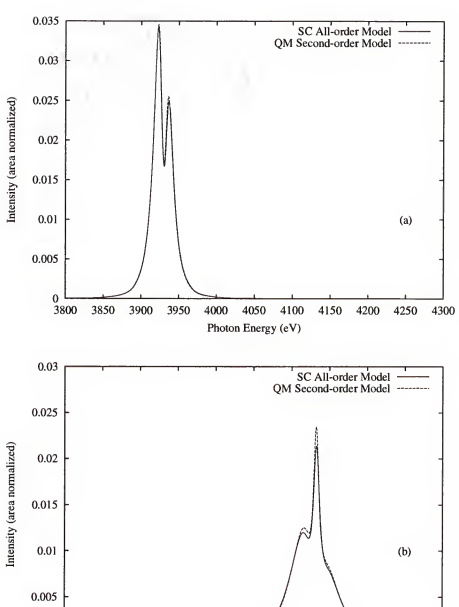

Figure 4.7: This figure shows comparisons of hydrogen-like argon spectra from the full-Coulomb SC and QM models at an electron density and temperature of 1×10^{24} cm^{-3} and 1 keV, respectively. Note that the two models are in good agreement for these line shapes. a) This plot shows the Lyman-β line of Ar^{+17}. b) This plot shows the Lyman-γ line of Ar^{+17}.

the density at 1×10^{24} cm^{-3} and lower the temperature to 600 eV, we see from Figure 4.9 that the full-Coulomb SC and QM models are still in good agreement. However, their are some minor differences in the width and shift of the lines. In fact, we do not see any significant differences between the models until the temperature drops to or below 400 eV, as is seen in Figure 4.10 and the corresponding semilog plot in Figure 4.11. Note that the wings of the line are beginning to differ significantly in the semilog figure. According to the conditions set forth by Cooper, Kelleher, and Lee [45]

$$k_B T > \frac{Z(Z-1)}{n^2} \text{Ryd} \tag{4.1}$$

the temperature limit for a second-order calculation is 460 eV for a Lyman-β line and 260 eV for a Lyman-γ line. This condition states that the momentum of the perturbing electron must be much larger than any change in its momentum. If this condition is violated, it basically means that strong collisions are becoming important in the determination of the line profile.

For perturbing electrons which penetrate the orbitals of the radiator and result in large shifts and distortions in the line profiles, we see that the SC all-order model and the QM second-order model still tend to agree with one another in the amount of shift and distortion over a wide range of temperatures. This agreement might seem odd because electron collisions which penetrate the orbital may seem to be strong. However, the strength of an electron collision depends on the duration of the collision and the electron's proximity to the radiator. The duration of the collision is an important factor because the electron speeds up as it passes by the radiator, thus decreasing the amount of time during which it interacts with the radiator. Therefore, fast electrons which penetrate the orbitals can still experience weak collisions, and thus the center region of the line shapes should be similar.

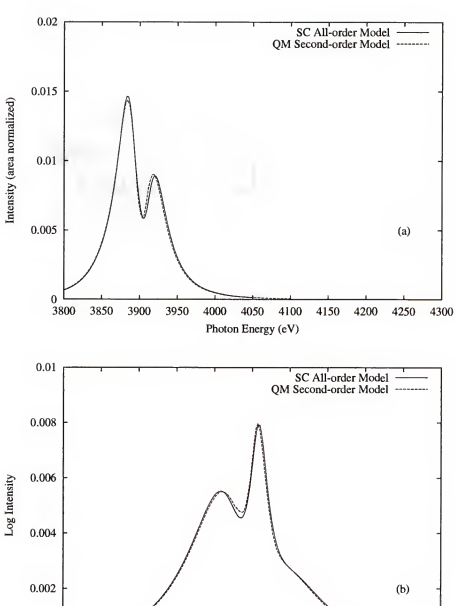

Figure 4.8: This figure shows comparisons of hydrogen-like argon spectra from the full-Coulomb SC all-order and QM second-order models at an electron density and temperature of 5×10^{24} cm^{-3} and 1 keV, respectively. Note that the two models are still in good agreement at this density. a) This plot shows the Lyman-β line of Ar^{+17}. b) This plot shows the Lyman-γ line of Ar^{+17}.

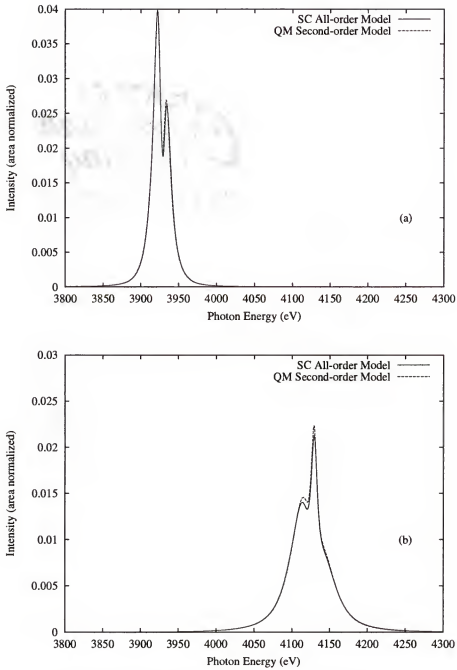

Figure 4.9: This figure shows comparisons of hydrogen-like argon spectra from the full-Coulomb SC all-order and QM second-order models at an electron density and temperature of 1×10^{24} cm^{-3} and 600 eV, respectively. Note that the two models are still in good agreement at this temperature. a) This plot shows the Lyman-β line of Ar^{+17}. b) This plot shows the Lyman-γ line of Ar^{+17}.

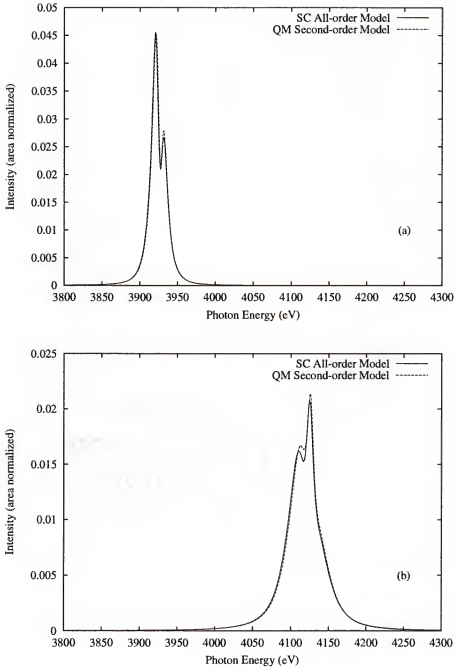

Figure 4.10: This figure shows comparisons of hydrogen-like argon spectra from the full-Coulomb SC all-order and QM second-order models at an electron density and temperature of 1×10^{24} cm^{-3} and 400 eV, respectively. Note that the two models are beginning to diverge in accordance with the temperature limit. a) This plot shows the Lyman-β line of Ar^{+17}. b) This plot shows the Lyman-γ line of Ar^{+17}.

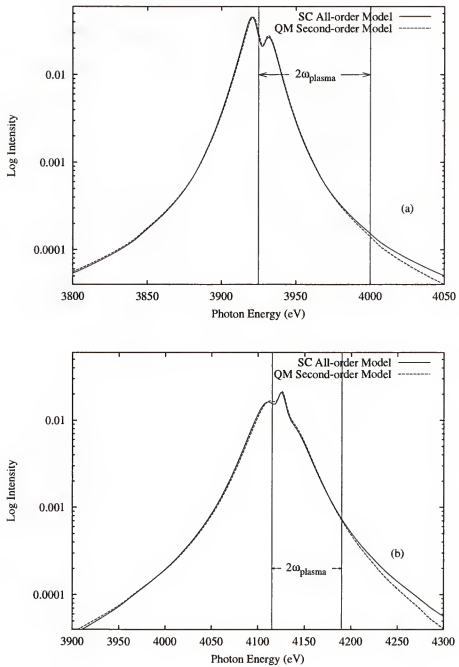

Figure 4.11: This figure shows comparisons of hydrogen-like argon spectra from the full-Coulomb SC all-order and QM second-order models on a semi-log plot at an electron density and temperature of 1×10^{24} cm^{-3} and 400 eV, respectively. Note that the two models are beginning to diverge in the wings when $\Delta\omega \gtrsim 2\omega_{plasma}$. Also, the energy scales are not the same on the two plots for reasons of comparison. a) This plot shows the Lyman-β line of Ar^{+17}. b) This plot shows the Lyman-γ line of Ar^{+17}.

We have shown that the results of the all-order theory and the second-order theory are generally in agreement. Now, we consider cases in which the SC all-order model is needed because the results of this model begin to show deviations from the results of a QM second-order model. Remember that in addition to the temperature limit imposed on the second-order model in Equation 4.1, the second-order model also begins to break down when $\Delta\omega \gtrsim 2\omega_{plasma}$. For example, look at the semilog plots in Figure 4.11. Because $\omega_{plasma} \approx 37$ eV at a density of 1×10^{24} cm^{-3}, we see that most of the difference occurs out in the wings of the line shape beyond $2\omega_{plasma}$ from line center. Also, low-Z radiators, such as hydrogenic helium, can emit spectral lines, for example Balmer lines, that have overall widths much larger than twice the plasma frequency. This limit can also be violated when attempting to calculate adjacent lines of a Rydberg series simultaneously. This type of calculation is required when considering the merging of two of more spectral lines.

As the width and especially the shift of the spectra in a Rydberg series increases with both increasing electron density and increasing principal quantum number, the n^{th} member of this series shifts toward the $(n-1)^{th}$ member. When the electron density becomes large enough, the Stark splitting of adjacent energy levels due to the ion microfield, together with the plasma induced shift in the lines, cause these series members to begin merging. As this happens, the theoretical spectra for both the n^{th} and $(n-1)^{th}$ members of the Rydberg series can no longer be calculated independently of one another. Off-diagonal matrix elements between the upper states of the n^{th} and $(n-1)^{th}$ spectral series members are on the order of the diagonal matrix elements, and mixing between the upper states of these series members is significant. For example, the magnitude of the matrix element $B_{4p,5p}$ is about half that of $B_{4p,4p}$. Because of this mixing, these series members merge together to form a composite spectral feature which does not obey a linear-shift model.

As evidence of the effect of mixing between the upper states of the Lyman β-, γ-, and δ-lines of Ar^{+17}, we show in Figure 4.12 a comparison of this composite feature with and without mixing between the upper-state manifolds using the SC all-order model with a full-Coulomb electron-radiator interaction at an electron density and temperature of $5 \times 10^{24} cm^{-3}$ and 1 keV, respectively. The calculation without mixing is often referred to as the linear model because we effectively are adding the intensities of the individual series members in which the density dependence of the shift of these members are nearly linear. A drawback of the linear model is that the shift of a Rydberg series member to lower energy increases with increasing principal quantum number and increases nearly linear with density, thus providing circumstances in which, for example, a δ-line can shift past a γ-line. The simultaneous calculation of the the Lyman series members with the inclusion of mixing destroys this linear shift dependence on the electron density, and thus is often referred to as the nonlinear model. The mixing between the upper-state manifolds of the Rydberg spectral series members in the nonlinear model prevents one member of a spectral series from shifting past another member.

Finally, let us consider differences between the SC all-order model and the QM second-order model using a full-Coulomb treatment of the electron-radiator interaction. Figures 4.13 and 4.14 show comparisons of the composite Lyman-$\beta\gamma\delta$ feature at the three different electron densities of 1×10^{24} cm^{-3}, 2.5×10^{24} cm^{-3}, and 5×10^{24} cm^{-3} with an electron temperature of 1 keV. As a reference, we also include the calculation of the linear SC all-order model in the figures. We see that as the electron density increases, the observable difference on the blue side of this composite feature increases and is large enough to be experimentally noticeable at densities near 5×10^{24} cm^{-3}. The difference shows that the SC all-order model predicts a process of merging which occurs more slowly with increasing electron density. The reason for this lies in the frequency-dependent resolvent in Equation B.8 of Appendix B. In the QM second-order theory mentioned in this work, the electron-radiator interaction term present in the denominator

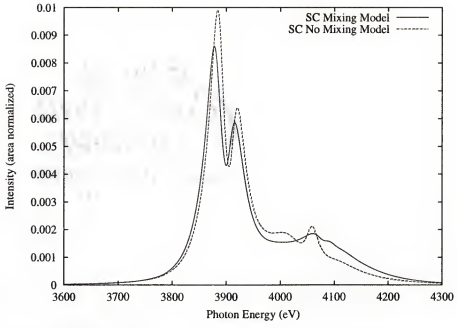

Figure 4.12: This figure shows the comparison of the theoretical Ar^{+17} Lyman-$\beta\gamma\delta$ feature calculated with the full-Coulomb SC all-order model with and without mixing between the upper-state manifolds of the individual lines at an electron density of 5×10^{24} cm^{-3} and an electron temperature of 1 keV.

is replaced by the first-order static shift. The reason for using this replacement instead of dropping the interaction term is that the value of this term approximates the contribution from the monopole part of $V^{(1)}_{1e,r}$. This term can be of a sufficiently large value such that it cannot be treated as a perturbation. Therefore, the QM second-order theory depends on a resolvent, and thus a time development operator, which is independent of the dynamic nature of the perturbing electron-radiator interaction $V^{(1)}_{1e,r}$. This, in turn, underestimates the dynamic behavior of the mixing between the upper states and overestimates the rate at which the members of the series merge together as the electron density increases.

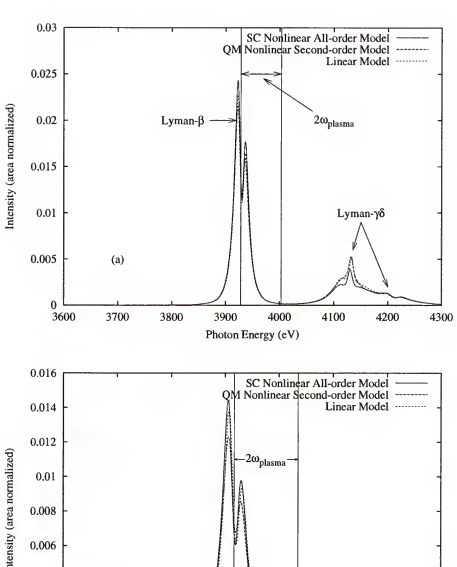

Figure 4.13: This figure shows the comparison of the theoretical composite Lyman-$\beta\gamma\delta$ feature of Ar^{+17} using the nonlinear, full-Coulomb SC all-order model (includes mixing), the nonlinear, full-Coulomb QM second-order model (includes mixing), and the full-Coulomb linear calculation (no mixing) which is nearly identical in both QM and SC models at a temperature of 1 keV over the density range shown. a) The spectra are calculated at an electron density of 1×10^{24} cm^{-3}. b) The spectra are calculated at an electron density of 2.5×10^{24} cm^{-3}.

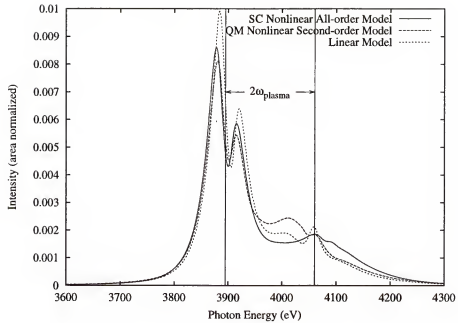

Figure 4.14: This figure shows the comparison of the theoretical composite Lyman-$\beta\gamma\delta$ feature of Ar^{+17} using the nonlinear, full-Coulomb SC all-order model (includes mixing), the nonlinear, full-Coulomb QM second-order model (includes mixing), and the full-Coulomb linear calculation (no mixing) which is nearly identical in both QM and SC models at an electron density and temperature of 1×10^{24} cm^{-3} and 1 keV, respectively.

CHAPTER 5
CONCLUSIONS

In this dissertation, we presented a semiclassical, all-order, full-Coulomb electron-broadening model which includes the effects of strong collisions through the inclusion of the terms to higher-order in the electron-radiator interaction. To calculate theoretical spectra for higher-Z radiators and to include contributions from strong collisions, we developed a model that differs from the VCS charged radiator model in these important ways:

- The interaction between the perturbing electron and the radiator is calculated using a multipole, or full-Coulomb calculation.
- Relativistic wavefunctions and the corresponding energy level structure from a relativistic atomic physics package are employed to describe the atomic physics of higher-Z radiators.
- A minimum separation cutoff is incorporated into the model. This cutoff is the Landau length modified by the radiator charge and quantum diffraction effects. The cutoff corrects for the singularity caused by the treatment of the electrons as classical particles.
- The distribution function is generalized to provide temperature-dependent changes in the relative populations of the radiator states modified by the interaction between the perturbing electron and the radiator.
- The no-quenching approximation, which prohibits nonradiative transitions caused by perturbations between states of differing principle quantum number n, must be relaxed to allow for nonradiative transitions between upper states of spectral lines which are beginning to merge together.

The results of this model were compared with a quantum mechanical, second-order, full-Coulomb electron-broadening model which does not treat strong collisions as thoroughly as our model does due to the exclusion of the higher-order terms. We considered the impact of strong-collision effects through the higher-order terms on line merging and other related physical phenomenon.

We discovered that the inclusion of strong-collision effects through the higher-order terms in the interaction can have a significant effect on the frequency dependence of

the width calculation in the wings of a line profile emitted by highly ionized, mid-Z radiators. It also has a significant effect on how quickly line profiles merge together as the density increases. As was shown, the spectral lines from the all-order model tend to merge more slowly than the line profiles from the second-order model.

As electron densities in inertial confinement fusion plasmas increase, this model has the potential to be useful as a tool in plasma spectroscopy diagnostics. As densities become sufficiently high, line profiles begin to merge together, and the shape of the composite feature seems to have a significant dependence on strong-collision effects through the inclusion of the higher-order terms. Also, the dipole approximation has been shown to be inadequate at higher electron densities where line shifts and line merging are important. This makes sense, because most of the strong-collision effects occur through the monopole interaction of the electron-radiator interaction when the perturbing electron penetrates the orbitals of a mid-Z radiator. These results are significant because plasma diagnostics may be extended to higher densities as researchers work to achieve "break even" energy creation in fusion research.

Differences in merged spectral lines due to strong collisions have the possibility of altering what we perceive as the distinction between continuum and bound states. Because ionization balance is sensitive to any changes in the energy level structure [28–30] and opacity is sensitive to the energy location and intensity of line emission, an understanding of the effects of strong collisions on the merged composite spectral features which lie near the continuum edge can be important.

Even at lower densities, we have shown that the frequency dependence of the width in the wings of a line profile are significantly dependent on the effects of strong collisions through the higher-order terms. This can have significant effects on Rosseland group opacities [31]. They are very sensitive to changes in the intensity of the line profile in the wings because they are proportional to a harmonic mean of the absorption coefficient. Rosseland group opacities, in turn, are important in the calculation of multi-group

diffusion radiative transfer effects. These effects, which are important in determining the amount of radiation that passes through different portions of the frequency spectrum, can be of importance in both astrophysical studies and in fusion research.

There are areas that need further examination in this model. First, as the density in the plasma increases, the one-electron approximation, where we allow only one strong electron collision with the radiator at a time along with the treatment of electron correlations through a static Debye shielding model, become questionable and therefore requires a more rigorous treatment. Second, in order to calculate spectral lines which have more than one final state, the model must be generalized to include lower-state broadening in addition to upper-state broadening. Third, the plasma electrons do not interact with the radiator in isolation with the presence of nearby ions, thus requiring at least a calculation of the width-and-shift operator in the presence of the ion electric microfield. Fourth, an examination of the quantum effects of intermediate momentum states of the perturbing electrons on line merging should be performed. Finally, at this time, we do not have conclusive experimental evidence to confirm the behavior of line merging as predicted by the theoretical models as of yet. Our NLUF (National Laser User Facility) campaign is currently underway on the OMEGA laser with the intention of generating sufficiently high densities and temperatures by varying laser pulse shapes, fill pressures of the microballoon, and the thickness of the ablator. Preliminary results indicate electron densities somewhat above 2×10^{24} cm^{-3} and temperatures above 1.5keV, and some very preliminary fits suggest that the nonlinear models fit somewhat better than the linear model. Also, with the startup of the NIF (National Ignition Facility) laser in 2003, the increased laser energy on target should allow us to probe plasmas in higher temperature and density regimes and allow us to more conclusively test the models in question.

APPENDIX A
EQUATION OF MOTION FOR $\boldsymbol{D}(\omega, \boldsymbol{\epsilon})$

In this appendix, we use Zwanzig's projection operator formalism [46] to derive the equation of motion for $\boldsymbol{D}(\omega, \boldsymbol{\epsilon})$. We then interpret the physical meaning of each of the terms in the equation of motion. From these terms, we then develop a model for both ion broadening and electron broadening of the spectral line shape.

To calculate the Stark-broadened line shape, we need to derive the equation of motion for Equation 2.22

$$\boldsymbol{D}(\omega, \boldsymbol{\epsilon}) = \frac{1}{Q(\boldsymbol{\epsilon})} \int_0^\infty \mathrm{d}t \; e^{\mathrm{i}(\omega - \mathrm{i}\epsilon)t} \, \mathrm{Tr}_p \left\{ \delta\left(\boldsymbol{\epsilon} - \boldsymbol{E}_{si}\right) \rho' e^{-\mathrm{i}H't/\hbar} \boldsymbol{d} \, e^{\mathrm{i}H't/\hbar} \right\} . \tag{A.1}$$

To simplify the form of this expression and the corresponding equation of motion, we apply the properties of a Liouville operator

$$L\hat{f} = \frac{1}{\hbar}\left[H', \hat{f}\right] \quad ; \quad e^{-\mathrm{i}Lt}\hat{f} = e^{-\mathrm{i}H't/\hbar}\hat{f}\, e^{\mathrm{i}H't/\hbar} \tag{A.2}$$

and perform the Laplace transform. Thus, $\boldsymbol{D}(\omega, \boldsymbol{\epsilon})$ becomes

$$\boldsymbol{D}(\omega, \boldsymbol{\epsilon}) = \frac{1}{Q(\boldsymbol{\epsilon})} \mathrm{Tr}_p \left\{ \delta\left(\boldsymbol{\epsilon} - \boldsymbol{E}_{si}\right) \rho' \frac{1}{(\omega - L)} \right\} \boldsymbol{d} . \tag{A.3}$$

In the application of the Zwanzig projection operator method, it useful to define

$$\rho'(\boldsymbol{\epsilon}) \equiv \frac{1}{Q(\boldsymbol{\epsilon})} \delta\left(\boldsymbol{\epsilon} - \boldsymbol{E}_{si}\right) \rho' \tag{A.4}$$

that is interpreted as the equilibrium state distribution function for a radiator immersed in a plasma constrained to have a microfield of the value $\boldsymbol{\epsilon}$. It is also useful to define

the Laplace transform of the time evolution of the radiator dipole as

$$\boldsymbol{X}(\omega) = \frac{1}{(\omega - L)}\,\boldsymbol{d} \tag{A.5}$$

so that $\boldsymbol{D}(\omega, \boldsymbol{\epsilon})$ now has the form

$$\boldsymbol{D}(\omega, \boldsymbol{\epsilon}) = \mathrm{Tr}_p \left\{ \rho'(\boldsymbol{\epsilon})\, \boldsymbol{X}(\omega) \right\} . \tag{A.6}$$

Utilizing the Zwanzig projection operator method, we can define the projection operator for the line broadening problem as having the action

$$PY = \int d\boldsymbol{\epsilon}\; \delta\left(\boldsymbol{\epsilon} - \boldsymbol{E}_{si}\right) \rho_{\boldsymbol{\epsilon},r}^{-1}\, \mathrm{Tr}_p \left\{ \rho'(\boldsymbol{\epsilon})\, Y \right\} \tag{A.7}$$

where

$$\rho_{\epsilon,\mathrm{r}} = \mathrm{Tr}_p\, \rho'(\boldsymbol{\epsilon}) \tag{A.8}$$

is the radiator reduced distribution function in the presence of the ion microfield. This projection operator selects the portion of the operator Y in the radiator-plasma system contributing to the ensemble average over the possible values of the ion microfield. Applying this projection operator to the operator $\boldsymbol{X}(\omega)$ as defined above, we have

$$P\boldsymbol{X}(\omega) = \int d\boldsymbol{\epsilon}\; \delta\left(\boldsymbol{\epsilon} - \boldsymbol{E}_{si}\right) \rho_{\boldsymbol{\epsilon},r}^{-1}\, \boldsymbol{D}(\omega, \boldsymbol{\epsilon}) . \tag{A.9}$$

Because P is a projection operator, it satisfies the relation $P^2 = P$. From the form of P, it is also easy to show that $P\boldsymbol{d} = \boldsymbol{d}$ because $\boldsymbol{d}$ does not depend on perturber coordinates. A projection operator of the form $Q = 1 - P$ picks out the portion of a system operator which is excluded when applying the projection operator P. We now use these two projection operators to derive the equation of motion for $\boldsymbol{D}(\omega, \boldsymbol{\epsilon})$. Applying

P to Equation A.5 and then Q to Equation A.5, we get a pair of equations

$$(\omega - PLP)\, P\boldsymbol{X} - (PLQ)\, Q\boldsymbol{X} = \boldsymbol{d} \tag{A.10}$$

$$(\omega - QLQ)\, Q\boldsymbol{X} - (QLP)\, P\boldsymbol{X} = 0 \tag{A.11}$$

By solving these two equations simultaneously, we find the equation of motion for $P\boldsymbol{X}$

$$\left(\omega - PLP - PLQ\,(\omega - QLQ)^{-1}\, QLP\right) P\boldsymbol{X} = \boldsymbol{d}\,. \tag{A.12}$$

Finally, by inserting the definition of the projection operator P into the equation of motion for $P\boldsymbol{X}$, we arrive at the formal equation of motion for $\boldsymbol{D}(\omega, \epsilon)$

$$\omega \boldsymbol{D}(\omega, \epsilon) - \int \mathrm{d}\epsilon' \left\{ B(\epsilon, \epsilon') + M(\epsilon, \epsilon'; \omega) \right\} \boldsymbol{D}(\omega, \epsilon') = \rho_{\epsilon, r} \boldsymbol{d} \tag{A.13}$$

where the instantaneous or static contributions to the broadening of the line shape are contained in the operator

$$B(\epsilon, \epsilon') = \mathrm{Tr}_p \left\{ \rho'(\epsilon) L\, \delta(\epsilon' - \boldsymbol{E}_{si}) \right\} \rho^{-1}_{\epsilon', r} \tag{A.14}$$

and the dynamic perturber collision contributions to the broadening of the line shape are contained in the operator

$$M(\epsilon, \epsilon'; \omega) = \mathrm{Tr}_p \left\{ \rho'(\epsilon) LQ \frac{1}{\omega - QLQ} QL\, \delta(\epsilon' - \boldsymbol{E}_{si}) \right\} \rho^{-1}_{\epsilon', r}\,. \tag{A.15}$$

The dynamic broadening operator $M(\epsilon, \epsilon'; \omega)$ is very complicated. Therefore, to illustrate the method at hand, we begin by analyzing the contributions to the

instantaneous broadening operator $B(\boldsymbol{\epsilon}, \boldsymbol{\epsilon}')$. Inserting the definition of $\rho'(\boldsymbol{\epsilon})$, we have

$$B(\boldsymbol{\epsilon}, \boldsymbol{\epsilon}') = \frac{1}{Q(\boldsymbol{\epsilon})} \mathrm{Tr}_p \left\{ \delta(\boldsymbol{\epsilon} - \boldsymbol{E}_{si}) \rho' L \, \delta(\boldsymbol{\epsilon}' - \boldsymbol{E}_{si}) \right\} \rho^{-1}_{\boldsymbol{\epsilon}', r} \,. \tag{A.16}$$

This expression can be rewritten in the form

$$\begin{aligned} B(\boldsymbol{\epsilon}, \boldsymbol{\epsilon}') \;=\; & \frac{1}{Q(\boldsymbol{\epsilon})} \mathrm{Tr}_p \left\{ L \, \delta(\boldsymbol{\epsilon} - \boldsymbol{E}_{si}) \rho' \delta(\boldsymbol{\epsilon}' - \boldsymbol{E}_{si}) \right\} \rho^{-1}_{\boldsymbol{\epsilon}', r} \\ & - \frac{1}{Q(\boldsymbol{\epsilon})} \mathrm{Tr}_p \left\{ [L \delta(\boldsymbol{\epsilon} - \boldsymbol{E}_{si})] \, \rho' \delta(\boldsymbol{\epsilon}' - \boldsymbol{E}_{si}) \right\} \rho^{-1}_{\boldsymbol{\epsilon}', r} \end{aligned} \tag{A.17}$$

because L does not commute with $\delta(\boldsymbol{\epsilon} - \boldsymbol{E}_{si})$. Substituting in the terms of the Liouville operator, this expression can be shown to have the form

$$B(\boldsymbol{\epsilon}, \boldsymbol{\epsilon}') = \delta(\boldsymbol{\epsilon} - \boldsymbol{\epsilon}') \left[L_r + \frac{1}{Q(\boldsymbol{\epsilon})} \mathrm{Tr}_p \left\{ L_I \delta(\boldsymbol{\epsilon} - \boldsymbol{E}_{si}) \right\} \rho^{-1}_{\boldsymbol{\epsilon}, r} \right] . \tag{A.18}$$

The contribution to L_I from the dipole interaction for both electrons and ions can be separated off and together give the Stark broadening operator, where $\mathbf{E}_{si}$ is identified as the ion field screened by the electrons [47]. Therefore,

$$B(\boldsymbol{\epsilon}, \boldsymbol{\epsilon}') = \delta(\boldsymbol{\epsilon} - \boldsymbol{\epsilon}') \left[L_r + L_{i,r}(\boldsymbol{\epsilon}) + B_e(\boldsymbol{\epsilon}) \right] \tag{A.19}$$

where

$$B_e(\boldsymbol{\epsilon}) = \frac{1}{Q(\boldsymbol{\epsilon})} \mathrm{Tr}_p \left\{ L^{(1)''}_{e,r} \delta(\boldsymbol{\epsilon} - \boldsymbol{E}_{si}) \rho' \right\} \rho^{-1}_{\boldsymbol{\epsilon}, r} \tag{A.20}$$

is the part of the instantaneous broadening operator containing the mean field effects of the perturbing electrons on the radiator. The primes on $L^{(1)''}_{e,r}$ correspond to the electron-radiator interaction minus the monopole and dipole contributions. Thus, the equation of motion, which is still exact, now has the form

$$[\omega - L_r - L_{i,r}(\boldsymbol{\epsilon}) - B_e(\boldsymbol{\epsilon})] \, \boldsymbol{D}(\omega, \boldsymbol{\epsilon}) - \int \mathrm{d}\boldsymbol{\epsilon}' M(\boldsymbol{\epsilon}, \boldsymbol{\epsilon}'; \omega) \boldsymbol{D}(\omega, \boldsymbol{\epsilon}') = \rho_{\boldsymbol{\epsilon}, r} \boldsymbol{d} \,. \tag{A.21}$$

As was noted above, the analysis of $M(\boldsymbol{\epsilon}, \boldsymbol{\epsilon}'; \omega)$ is more complex and can be done qualitatively as follows. First, note that the appearance of QL assures that only the interaction parts of L occur (i.e., $QL \rightarrow QL_I$). Thus, $M(\boldsymbol{\epsilon}, \boldsymbol{\epsilon}'; \omega)$ has contributions describing broadening by ion dynamics, electron dynamics, and cross terms representing their correlation. As a first approximation, we assume that there are no dynamical correlations between the electrons and the ions. Therefore, it can be shown that

$$M(\boldsymbol{\epsilon}, \boldsymbol{\epsilon}'; \omega) \rightarrow M_i(\boldsymbol{\epsilon}, \boldsymbol{\epsilon}'; \omega) + \delta(\boldsymbol{\epsilon} - \boldsymbol{\epsilon}') M_e(\omega, \boldsymbol{\epsilon}) \tag{A.22}$$

where $M_i(\boldsymbol{\epsilon}, \boldsymbol{\epsilon}'; \omega)$ and $M_e(\boldsymbol{\epsilon}; \omega)$ describe the dynamical effects of the ions and electrons, respectively. Using this approximation, the equation of motion has the form

$$\begin{aligned} &[\omega - L_r - L_{i,r}(\boldsymbol{\epsilon}) - B_e(\boldsymbol{\epsilon}) - M_e(\omega, \boldsymbol{\epsilon})]\, \boldsymbol{D}(\omega, \boldsymbol{\epsilon}) \\ &\qquad - \int \mathrm{d}\boldsymbol{\epsilon}'\, M_i(\boldsymbol{\epsilon}, \boldsymbol{\epsilon}'; \omega) \boldsymbol{D}(\omega, \boldsymbol{\epsilon}') = \rho_{\boldsymbol{\epsilon},r} \boldsymbol{d} \end{aligned} \tag{A.23}$$

which is quoted and discussed in the text, noting that the various broadening mechanisms have been isolated and identified.

Using an ion motion assumption in which the transitions among different field values are instantaneous and uncorrelated (Poisson process), the ion-dynamics collision term can be written in the form [38]

$$\begin{aligned} \int \mathrm{d}\boldsymbol{\epsilon}'\, M_i(\boldsymbol{\epsilon}, \boldsymbol{\epsilon}'; \omega) \boldsymbol{D}(\omega, \boldsymbol{\epsilon}') &= \mathrm{i}\nu \rho_{\boldsymbol{\epsilon},r} \int \mathrm{d}\boldsymbol{\epsilon}' Q(\boldsymbol{\epsilon}') \left\{ \rho^{-1}_{\boldsymbol{\epsilon}',r} \boldsymbol{D}(\omega, \boldsymbol{\epsilon}) - \rho^{-1}_{\boldsymbol{\epsilon}',r} \boldsymbol{D}(\omega, \boldsymbol{\epsilon}') \right\} \\ &= \mathrm{i}\nu \boldsymbol{D}(\omega, \boldsymbol{\epsilon}) - \mathrm{i}\nu \rho_{\boldsymbol{\epsilon},r} \int \mathrm{d}\boldsymbol{\epsilon}' Q(\boldsymbol{\epsilon}') \rho^{-1}_{\boldsymbol{\epsilon}',r} \boldsymbol{D}(\omega, \boldsymbol{\epsilon}') \end{aligned} \tag{A.24}$$

where ν is directly proportional to the momentum autocorrelation function of the ions and is a measure of the importance of ion motion effects on the line shape. With this

definition, we see that $\rho_{\epsilon,r}$ is a stationary point of M_i, or

$$\int \mathrm{d}\epsilon' M_i(\epsilon, \epsilon'; \omega)\rho_{\epsilon',r} = 0\,. \tag{A.25}$$

Now, if we define

$$G(\omega, \epsilon) = \frac{1}{\omega - L_r - L_{i,r}(\epsilon) - B_e(\epsilon) - M_e(\omega, \epsilon) - \mathrm{i}\nu}\,, \tag{A.26}$$

the equation of motion for $\boldsymbol{D}(\omega, \epsilon)$ has the form

$$\boldsymbol{D}(\omega, \epsilon) = G(\omega, \epsilon)\left[\rho_{\epsilon,r}\boldsymbol{d} - \mathrm{i}\nu\rho_{\epsilon,r}\int \mathrm{d}\epsilon' Q(\epsilon')\rho^{-1}_{\epsilon',r}\boldsymbol{D}(\omega, \epsilon')\right]\,. \tag{A.27}$$

Next, we solve the equation of motion and find an expression for $\boldsymbol{D}(\omega, \epsilon)$. By defining the quantity $\boldsymbol{Y}$ as

$$\boldsymbol{Y} \equiv \int \mathrm{d}\epsilon' Q(\epsilon')\rho^{-1}_{\epsilon',r}\boldsymbol{D}(\omega, \epsilon') \tag{A.28}$$

and substituting Equation A.27 into $\boldsymbol{Y}$, we have

$$\boldsymbol{Y} = \int \mathrm{d}\epsilon' Q(\epsilon')\rho^{-1}_{\epsilon',r}G(\omega, \epsilon')\left[\rho_{\epsilon',r}\boldsymbol{d} - \mathrm{i}\nu\rho_{\epsilon',r}\boldsymbol{Y}\right]\,. \tag{A.29}$$

Solving this expression for $\boldsymbol{Y}$, we find that

$$\boldsymbol{Y} = \frac{1}{1 + \mathrm{i}\nu\int \mathrm{d}\epsilon' Q(\epsilon')\rho^{-1}_{\epsilon',r}G(\omega, \epsilon')\rho_{\epsilon',r}}\int \mathrm{d}\epsilon' Q(\epsilon')\rho^{-1}_{\epsilon',r}G(\omega, \epsilon')\rho_{\epsilon',r}\boldsymbol{d}\,. \tag{A.30}$$

By noting the definition of $\boldsymbol{Y}$ and substituting this expression into Equation A.27, we find that after some simple reduction

$$\boldsymbol{D}(\omega, \epsilon) = G(\omega, \epsilon)\rho_{\epsilon,r}\frac{1}{1 + \mathrm{i}\nu\int \mathrm{d}\epsilon' Q(\epsilon')\rho^{-1}_{\epsilon',r}G(\omega, \epsilon')\rho_{\epsilon',r}}\,\boldsymbol{d}\,. \tag{A.31}$$

Also, from the definition of $\rho_{\epsilon',r}$, it can be shown that

$$G(\omega,\epsilon') = \rho^{-1}_{\epsilon',r} G(\omega,\epsilon')\rho_{\epsilon',r} \tag{A.32}$$

that is then used to arrive at the final expression for $\boldsymbol{D}(\omega,\epsilon)$ used in the text. This final expression has the form

$$\boldsymbol{D}(\omega,\epsilon) = G(\omega,\epsilon)\rho_{\epsilon,r}\frac{1}{1+i\nu\int d\epsilon' Q(\epsilon')G(\omega,\epsilon')}\,\boldsymbol{d}. \tag{A.33}$$

APPENDIX B
ELECTRON-BROADENING OPERATOR

From Appendix A, we found that the instantaneous or static contribution to the electron-broadening operator has the form

$$B_e(\epsilon) = \frac{1}{Q(\epsilon)} \mathrm{Tr}_e \left\{ L_{e,r}^{(1)''} \mathrm{Tr}_i \left[\delta(\epsilon - \boldsymbol{E}_{st}) \rho' \right] \right\} \rho_{e,r}^{-1} \tag{B.1}$$

In Appendix A, we also applied the approximation that there are no dynamical correlations between the ions and the electrons. Under this approximation, the dynamic portion of the electron-broadening operator has the form

$$M_e(\omega, \epsilon) = \mathrm{Tr}_e \left\{ \mathrm{Tr}_i \left[\rho'(\epsilon) \right] L_{e,r}^{(1)} Q \frac{1}{\omega - QL(\epsilon)Q} QL_{e,r}^{(1)} \right\} \rho_{e,r}^{-1} \tag{B.2}$$

where

$$L(\epsilon) = L_r + L_e + L_{i,r}(\epsilon) + L_{e,r}^{(1)} \tag{B.3}$$

describes the dynamics of the electron-radiator interactions. The presence of the projection operator Q under the current approximation selects the part of the occurrences of L in the numerator containing the the electron-radiator interaction, $L_{e,r}^{(1)}$. Also, L_r is the Liouville operator of the isolated radiator, L_e is the Liouville operator for the plasma electrons, and $L_{i,r}(\epsilon)$ is the Liouville operator for the ion Stark splitting. Note that the ion degrees of freedom have been integrated out because they have been assumed to be "static" in the electron-broadening operator.

By applying a weak-coupling approximation between the ions and the electrons which is given by

$$\rho' = \rho_{\epsilon,\epsilon,r} \rho_i \tag{B.4}$$

the static and dynamic parts of the electron-broadening operator now have the form

$$B_e(\boldsymbol{\epsilon}) = \mathrm{Tr}_e \left\{ L^{(1)}_{e,r}{}'' \rho_{e,\boldsymbol{\epsilon},r} \right\} \rho^{-1}_{\boldsymbol{\epsilon},r} \tag{B.5}$$

and

$$M_e(\omega,\boldsymbol{\epsilon}) = \mathrm{Tr}_e \left\{ \rho_{e,\boldsymbol{\epsilon},r} L^{(1)}_{e,r} Q \frac{1}{\omega - QL(\boldsymbol{\epsilon})Q} Q L^{(1)}_{e,r} \right\} \rho^{-1}_{\boldsymbol{\epsilon},r}. \tag{B.6}$$

Note that in this simplification, we have used the definition of the ion microfield probability distribution function, and $\rho_{e,\boldsymbol{\epsilon},r}$ is the reduced electron-radiator density matrix in the presence of the ion field $\boldsymbol{\epsilon}$.

We next apply a one-electron approximation in which we neglect electron correlations and simultaneous strong electron-radiator interactions by two or more electrons. Under this approximation, the occurrences of the projection operator Q vanish, and the static and dynamic parts of the electron-broadening operator now have the form

$$B(\boldsymbol{\epsilon}) = n_e \mathrm{Tr}_{1e} \{ L^{(1)}_{1e,r} \rho_{1e,\boldsymbol{\epsilon},r} \} \rho^{-1}_{\boldsymbol{\epsilon},r} \tag{B.7}$$

and

$$M(\omega,\boldsymbol{\epsilon}) = n_e \mathrm{Tr}_{1e} \left\{ L^{(1)}_{1e,r} \frac{1}{\omega - L_r(\boldsymbol{\epsilon}) - L_{1e} - L^{(1)}_{1e,r}} \rho_{1e,\boldsymbol{\epsilon},r} L^{(1)}_{1e,r} \right\} \rho^{-1}_{\boldsymbol{\epsilon},r} \tag{B.8}$$

where

$$L_r(\boldsymbol{\epsilon}) = L_r + L^{(1)}_{i,r}(\boldsymbol{\epsilon}) \,. \tag{B.9}$$

To compensate for the removal of electron correlations, we apply a Debye static shielding approximation to the calculation of the electron-broadening operator [39].

Next, we reformulate the expression for the dynamic electron collision operator in terms of a time development operator using the interaction representation. In the dynamic electron-broadening operator, the frequency dependent denominator contains all of the dynamic or time dependent properties of the electron collisions with the

radiator. Through an inverse Laplace transform, this resolvent term can be expressed as

$$\frac{1}{\omega - L_r(\boldsymbol{\epsilon}) - L_{1\epsilon} - L^{(1)}_{1\epsilon,r}} = -\mathrm{i}\int_0^\infty \mathrm{d}t\, e^{\mathrm{i}(\omega - L_r(\boldsymbol{\epsilon}) - L_{1\epsilon} - L^{(1)}_{1\epsilon,r} + \mathrm{i}\epsilon)t}. \tag{B.10}$$

However, because the electron broadening of the line shape is due to the perturbing electron-radiator interaction, it is advantageous to rewrite this quantity in the interaction representation. Therefore, the resolvent can be expressed in terms of a time development operator

$$\frac{1}{\omega - L_r(\boldsymbol{\epsilon}) - L_{1\epsilon} - L^{(1)}_{1\epsilon,r}} = -\mathrm{i}\int_0^\infty \mathrm{d}t\, e^{\mathrm{i}(\omega - L_r(\boldsymbol{\epsilon}) - L_{1\epsilon} + \mathrm{i}\epsilon)t}\, \mathcal{U}(t,0) \tag{B.11}$$

where

$$\mathcal{U}(t,0) = \vartheta \exp\left\{-\mathrm{i}\int_0^t \mathrm{d}t'\, \tilde{L}^{(1)}_{1\epsilon,r}(t')\right\} \tag{B.12}$$

and

$$\tilde{L}^{(1)}_{1\epsilon,r}(t) = e^{\mathrm{i}(L_r(\boldsymbol{\epsilon}) + L_{1\epsilon})t}\, L^{(1)}_{1\epsilon,r}\, e^{-\mathrm{i}(L_r(\boldsymbol{\epsilon}) + L_{1\epsilon})t}. \tag{B.13}$$

The time development operator and its dynamical properties are defined by the differential equation

$$\mathrm{i}\frac{\partial \mathcal{U}(t,0)}{\partial t} = \tilde{L}^{(1)}_{1\epsilon,r}(t)\mathcal{U}(t,0), \tag{B.14}$$

and ϑ represents a time-ordered treatment of the exponential similar to that seen in a Dyson expansion. With the substitution of the expression for the resolvent, the dynamic electron-broadening operator can be expressed as

$$\begin{aligned} M(\omega,\boldsymbol{\epsilon}) = -\mathrm{i}n_e \int_0^\infty \mathrm{d}t\, e^{\mathrm{i}(\omega - L_r(\boldsymbol{\epsilon}) + \mathrm{i}\epsilon)t}\, \mathrm{Tr}_{1\epsilon}\Big\{ & \tilde{L}^{(1)}_{1\epsilon,r}(t) \\ & \times \mathcal{U}(t,0)\, \rho_{1\epsilon,\boldsymbol{\epsilon},r}\, L^{(1)}_{1\epsilon,r}\Big\}\, \rho^{-1}_{\boldsymbol{\epsilon},r} \end{aligned} \tag{B.15}$$

where the invariance of the trace under a time translation of the perturbing electron coordinates has been used to simplify this operator.

Because we are interested specifically in radiative transitions between initial and final states, we now apply the no-quenching approximation. From Equation 2.27, it is observed that the width-and-shift operator acts on the radiator dipole moment $\boldsymbol{d}$. Under the no-quenching approximation, the matrix elements of the perturbing electron-radiator interaction between initial and final states of the transition are zero. This results in matrix elements only between initial and final states of the radiator transition for this occurrence of the radiator dipole moment, noted by $\boldsymbol{d}_{if}$. If we operate $B(\boldsymbol{\epsilon})$ and $M(\omega, \boldsymbol{\epsilon})$ on $\boldsymbol{d}_{if}$ and expand the commutator definitions of the Liouville operator, we then have

$$\begin{aligned} B(\boldsymbol{\epsilon})\boldsymbol{d}_{if} &= n_e \mathrm{Tr}_{1e}\{V^{(1)}_{1e,r}\,\rho_{1e,\boldsymbol{\epsilon},r}\,\rho^{-1}_{\boldsymbol{\epsilon},r}\boldsymbol{d}_{if}\} \\ &- n_e \mathrm{Tr}_{1e}\{\rho_{1e,\boldsymbol{\epsilon},r}\,\rho^{-1}_{\boldsymbol{\epsilon},r}\boldsymbol{d}_{if}\,V^{(1)}_{1e,r}\} \end{aligned} \tag{B.16}$$

and

$$\begin{aligned} M(\omega,\boldsymbol{\epsilon})\boldsymbol{d}_{if} &= -\mathrm{i}n_e \int_0^\infty \mathrm{d}t\, e^{\mathrm{i}(\omega - H_{\boldsymbol{\epsilon},r} + \mathrm{i}\epsilon)t}\,\mathrm{Tr}_{1e}\Big\{\tilde{V}^{(1)}_{1e,r}(t)\,U(t,0) \\ &\qquad \times \rho_{1e,\boldsymbol{\epsilon},r}\,V^{(1)}_{1e,r}\,\rho^{-1}_{\boldsymbol{\epsilon},r}\,\boldsymbol{d}_{if}\,U^\dagger(t,0)\Big\}\,e^{\mathrm{i}H_{\boldsymbol{\epsilon},r}t} \\ &+ \mathrm{i}n_e \int_0^\infty \mathrm{d}t\, e^{\mathrm{i}(\omega - H_{\boldsymbol{\epsilon},r} + \mathrm{i}\epsilon)t}\,\mathrm{Tr}_{1e}\Big\{U(t,0)\,\rho_{1e,\boldsymbol{\epsilon},r}\,V^{(1)}_{1e,r} \\ &\qquad \times \rho^{-1}_{\boldsymbol{\epsilon},r}\,\boldsymbol{d}_{if}\,U^\dagger(t,0)\,\tilde{V}^{(1)}_{1e,r}(t)\Big\}\,e^{\mathrm{i}H_{\boldsymbol{\epsilon},r}t} \\ &+ \mathrm{i}n_e \int_0^\infty \mathrm{d}t\, e^{\mathrm{i}(\omega - H_{\boldsymbol{\epsilon},r} + \mathrm{i}\epsilon)t}\,\mathrm{Tr}_{1e}\Big\{\tilde{V}^{(1)}_{1e,r}(t)\,U(t,0) \\ &\qquad \times \rho_{1e,\boldsymbol{\epsilon},r}\,\rho^{-1}_{\boldsymbol{\epsilon},r}\,\boldsymbol{d}_{if}\,V^{(1)}_{1e,r}\,U^\dagger(t,0)\Big\}\,e^{\mathrm{i}H_{\boldsymbol{\epsilon},r}t} \\ &- \mathrm{i}n_e \int_0^\infty \mathrm{d}t\, e^{\mathrm{i}(\omega - H_{\boldsymbol{\epsilon},r} + \mathrm{i}\epsilon)t}\,\mathrm{Tr}_{1e}\Big\{U(t,0)\,\rho_{1e,\boldsymbol{\epsilon},r}\,\rho^{-1}_{\boldsymbol{\epsilon},r} \\ &\qquad \times \boldsymbol{d}_{if}\,V^{(1)}_{1e,r}\,U^\dagger(t,0)\,\tilde{V}^{(1)}_{1e,r}(t)\Big\}\,e^{\mathrm{i}H_{\boldsymbol{\epsilon},r}t} \end{aligned} \tag{B.17}$$

The first term describes the broadening on the upper states of the transition, the last term describes the broadening on the lower states of the transition, and the two

intermediate terms in $M(\omega, \boldsymbol{\epsilon})$ are interference terms between upper and lower states. Because of the no-quenching approximation, operators to the left of $\boldsymbol{d}_{if}$ act on the initial-state manifold of the transition and operators to the right of $\boldsymbol{d}_{if}$ act on the final-state manifold of the transition.

Because this dissertation concentrates on line spectra which have no significant lower state broadening, we apply a no lower-state broadening approximation which is discussed in Chapter 3. Therefore, we concentrate on the first term of instantaneous part of the electron-broadening operator

$$B^{first}(\boldsymbol{\epsilon})\boldsymbol{d} = n_e \mathrm{Tr}_{1e}\{V^{(1)}_{1e,r}\,\rho_{1e,\epsilon,r}\}\,\rho^{-1}_{\boldsymbol{\epsilon},r}\boldsymbol{d} \tag{B.18}$$

and the first term of the dynamic part of the electron-broadening operator

$$\begin{aligned} M^{first}(\omega, \boldsymbol{\epsilon})\boldsymbol{d} = -\mathrm{i}n_e \int_0^\infty \mathrm{d}t\, e^{\mathrm{i}(\omega - H_{\epsilon,r} + \mathrm{i}\epsilon)t}\, \mathrm{Tr}_{1e}\Big\{ \tilde{V}^{(1)}_{1e,r}(t)\, U(t,0) \\ \times \rho_{1e,\epsilon,r}\, V^{(1)}_{1e,r}\, \rho^{-1}_{\boldsymbol{\epsilon},r}\, \boldsymbol{d}\, U^\dagger(t,0)\Big\}\, e^{\mathrm{i}H_{\epsilon,r}t}\,, \end{aligned} \tag{B.19}$$

where the time development operator has the form

$$U(t,0) = \vartheta \exp\left\{ -\mathrm{i}\int_0^t \mathrm{d}t'\, \tilde{V}^{(1)}_{1e,r}(t') \right\} \tag{B.20}$$

and

$$\tilde{V}^{(1)}_{1e,r}(t) = e^{\mathrm{i}(H_{\epsilon,r} + H'_{1e})t}\, V^{(1)}_{1e,r}\, e^{-\mathrm{i}(H_{\epsilon,r} + H'_{1e})t}\,. \tag{B.21}$$

The time development operator satisfies the differential equation

$$\mathrm{i}\hbar \frac{\partial U(t,0)}{\partial t} = \tilde{V}^{(1)}_{1e,r}(t) U(t,0)\,. \tag{B.22}$$

These are the expressions which are used in the main body of the text for the calculation of the line shapes of interest in this dissertation.

APPENDIX C
DEUTSCH POTENTIAL AND THE QUANTUM CUTOFF

In the model presented in this dissertation, we consider the case of electrons treated as classical particles undergoing collisions with a radiating ion which gives rise to broadening effects on the emitted spectral lines. However, under a classical treatment of the radiator-electron Coulomb interactions, the potential goes to negative infinity as the distance between the radiator and the electrons go to zero. In order to remove this singularity, a minimum distance cutoff is derived by applying quantum diffraction effects through the calculation of the pair potential introduced by Deutsch [40]. In this appendix, we sketch out the form of this pair potential. The pair potential is then used to define a minimum distance cutoff that used in the electron-broadening model presented in this dissertation.

The effective pair potential $V_{ij}(r)$ is defined as a function of the two-particle radial distribution function, $g_{ij}(r)$, by

$$V_{ij}(r) = -\mathrm{k_B}T \ln g_{ij}(r) . \tag{C.1}$$

For the radiator-electron interactions, the radial distribution function can be considered as the sum of contributions from bound and scattered states of the radiator

$$g_{ij}(r) = g_s(r) + g_b(r) . \tag{C.2}$$

The scattered state contribution can be written in terms of Coulomb wave functions $F_l(\alpha, kr)$

$$g_s(r) = \left(2\pi\lambda_{ij}^2\right)^{3/2} \frac{1}{4\pi r^2} \int_0^\infty \mathrm{d}k \; e^{\lambda_{ij}^2 k^2/2} \sum_{l=0}^{\infty} \frac{(2l+1)^2}{l+1/2} |F_l(\alpha, kr)|^2 \tag{C.3}$$

where λ_{ij} is the thermal De Broglie wavelength

$$\lambda_{ij} = \left(\frac{\hbar^2}{2\mu_{ij} \mathrm{k_B} T}\right)^{1/2} \tag{C.4}$$

and

$$\alpha = \frac{-Ze^2\mu_{ij}}{\hbar^2 k}. \tag{C.5}$$

Z is the overall charge of the radiating ion and μ_{ij} is the reduced mass of the electron-radiator pair, which is effectively equal to the electron mass for most cases of interest. The bound state contributions can be written in terms of the bound state wave functions of the radiator $\psi_{nlm}(r, \theta, \phi)$

$$g_b(r) = \left(2\pi\lambda_{ij}^2\right)^{3/2} \frac{1}{4\pi} \iint \sin\theta \, \mathrm{d}\theta \, \mathrm{d}\phi \sum_{n,l,m} |\psi_{nlm}(r, \theta, \phi)|^2. \tag{C.6}$$

We now define the minimum distance cutoff used in the calculation of the electron-broadening operator as

$$r_{min} \equiv r \frac{V_C(r)}{V_{ij}(r)} \tag{C.7}$$

where $V_C(r)$ is the bare Coulomb potential between the radiator and the electron. Substituting in the definitions for the potentials, we have

$$r_{min} = \frac{Z \, r_{lnd}}{\ln g_{ij}(r \to 0)} \tag{C.8}$$

where r_{lnd} is the Landau length

$$r_{lnd} = \frac{e^2}{k_B T} . \tag{C.9}$$

The use of $Z\, r_{lnd}$ as the cutoff would effectively limit the strength of the perturbing electron-radiator interaction to approximately

$$\left| V^{(1)}_{1e,r} \right|_{max} \sim \frac{k_B T}{Z} \tag{C.10}$$

and assures that the strength of the interaction is balanced by the speed of the electron as it passes by the charged radiator. Also, note that $\ln g_{ij}(r \to 0)$ modifies the cutoff for quantum diffraction effects between the perturbing electron and the radiator [40] because there is overlap of the wave packet of the perturbing electron with the radiator orbitals.

APPENDIX D
IRREDUCIBLE TENSOR OPERATORS AND 3N-J SYMBOLS

This appendix provides a brief overview of a formalism that is very useful for the treatment of angular momentum dependent matrix elements. These definitions, identities, and sum rules are be employed in the calculation of the matrix elements of the perturbing electron-radiator interaction. First, Wigner 3N-j symbols [43,48,49] are introduced in terms of an integral over spherical harmonics,

$$\int_0^{2\pi}\int_0^{\pi} Y^*_{lm}Y_{kq}Y_{l'm'}sin\theta d\theta d\phi = (-1)^m\left(\frac{[l,k,l']}{4\pi}\right)^{\frac{1}{2}}\begin{pmatrix} l & k & l' \\ -m & q & m' \end{pmatrix}\begin{pmatrix} l & k & l' \\ 0 & 0 & 0 \end{pmatrix}, \tag{D.1}$$

where

$$[l,l',\ldots] = (2l+1)(2l'+1)\cdots . \tag{D.2}$$

There are several useful relations and symmetry properties that are employed in this work, such as

$$\begin{pmatrix} j_2 & j_1 & j_3 \\ m_2 & m_1 & m_3 \end{pmatrix} = (-1)^{j_1+j_2+j_3}\begin{pmatrix} j_1 & j_2 & j_3 \\ m_1 & m_2 & m_3 \end{pmatrix}, \tag{D.3}$$

and

$$\begin{pmatrix} j_1 & j_2 & j_3 \\ -m_1 & -m_2 & -m_3 \end{pmatrix} = (-1)^{j_1+j_2+j_3}\begin{pmatrix} j_1 & j_2 & j_3 \\ m_1 & m_2 & m_3 \end{pmatrix}. \tag{D.4}$$

The following relation can be obtained using the orthogonality of spherical harmonic functions,

$$\begin{pmatrix} j & j' & 0 \\ m & -m' & 0 \end{pmatrix} = (-1)^{j-m}[j]^{-1/2}\delta_{jj'}\delta_{mm'}. \tag{D.5}$$

Also, the equation $m_1 + m_2 + m_3 = 0$ must be satisfied for a 3-j symbol to be nonzero. He are several useful sum rules:

$$\sum_{j_3}\sum_{m_3}[j_3]\begin{pmatrix} j_1 & j_2 & j_3 \\ m_1 & m_2 & m_3 \end{pmatrix}\begin{pmatrix} j_1 & j_2 & j_3 \\ m_1' & m_2' & m_3 \end{pmatrix} = \delta_{m_1m_1'}\delta_{m_2m_2'}, \tag{D.6}$$

$$\sum_{m_1}\sum_{m_2}[j_3]\begin{pmatrix} j_1 & j_2 & j_3 \\ m_1 & m_2 & m_3 \end{pmatrix}\begin{pmatrix} j_1 & j_2 & j_3' \\ m_1 & m_2 & m_3' \end{pmatrix} = \delta_{j_3j_3'}\delta_{m_3m_3'}\delta(j_1j_2j_3), \tag{D.7}$$

and,

$$\sum_{m}(-1)^{j-m}\begin{pmatrix} j & j & j_3 \\ m & -m & 0 \end{pmatrix} = \delta_{j_30}[j]^{1/2}, \tag{D.8}$$

where $\delta(j_1j_2j_3)$ is $+1$ if the triangle relations are satisfied.

The Wigner-Eckart Theorem [41,42] is employed to express the matrix elements of our interaction potential in terms of reduced matrix elements as follows:

$$\langle \alpha jm|T_q^{(k)}|\alpha' j'm'\rangle = (-1)^{j-m}\begin{pmatrix} j & k & j' \\ m & q & -m' \end{pmatrix}\langle \alpha j||T^{(k)}||\alpha' j'\rangle, \tag{D.9}$$

where $T_q^{(k)}$ is an irreducible tensor operator, j and j' are the angular momentum indices of the coordinates relevant to the operator, and α and α' represent all the other quantities (energy, spin, etc.) that define their respective states.

A particular example of reduced matrix elements that is employed is the matrix elements of spherical harmonics. The angular portion of our perturbing electron-radiator

interaction is written in terms of normalized spherical harmonics, defined as,

$$C_q^{(k)}(\theta,\phi) = \left(\frac{4\pi}{[k]}\right)^{1/2} Y_{kq}(\theta,\phi). \tag{D.10}$$

Several relations pertaining to reduced matrix elements of spherical harmonics are written below:

$$\langle l||C^{(k)}||l'\rangle = (-1)^l [l,l']^{1/2} \begin{pmatrix} l & k & l' \\ 0 & 0 & 0 \end{pmatrix}, \tag{D.11}$$

$$\langle \alpha l||C^{(0)}||\alpha l'\rangle = [l]^{1/2}\delta_{\alpha,\alpha'}\delta_{l,l'}, \tag{D.12}$$

and

$$\langle l'||C^{(k)}||l\rangle = (-1)^k \langle l||C^{(k)}||l'\rangle. \tag{D.13}$$

6-j symbols are also used to evaluate the angular portions of the matrix elements. The symbols are defined as follows:

$$\begin{Bmatrix} j_1 & j_2 & j_3 \\ l_1 & l_2 & l_3 \end{Bmatrix} = [j_3] \sum_{m_1 m_2} \sum_{n_1 n_2 n_3} \begin{pmatrix} j_1 & j_2 & j_3 \\ m_1 & m_2 & m_3 \end{pmatrix} \begin{pmatrix} j_1 & l_2 & l_3 \\ m_1 & n_2 & -n_3 \end{pmatrix} \begin{pmatrix} l_1 & j_2 & l_3 \\ -n_1 & m_2 & n_3 \end{pmatrix} \begin{pmatrix} l_1 & l_2 & j_3 \\ n_1 & -n_2 & m_3 \end{pmatrix}, \tag{D.14}$$

With regard to symmetry properties, a 6-j symbol is unchanged when any two columns are interchanged and if any two numbers in the bottom row are interchanged with the corresponding two numbers in the top row. The arguments in the top row must satisfy a triangle relation,

$$|j_2 - j_3| \le j_1 \le j_2 + j_3, \quad |j_1 - j_3| \le j_2 \le j_1 + j_3, \quad |j_1 - j_2| \le j_3 \le j_1 + j_2, \tag{D.15}$$

and their sum must be a positive integer for the 6-j symbol to be nonzero. Also, any set of arguments that can be permuted into the top row must also satisfy these conditions.

REFERENCES

[1] H. Griem, *Principles of Plasma Spectroscopy* (Cambridge University Press, Cambridge, UK, 1997).

[2] R. Breene, Jr., *Theories of Spectral Line Shape* (Benjamin Cummings Publishing, Menlo Park, CA, 1981).

[3] C. Hooper, Jr., Phys. Rev. Lett. **63**, 267 (1989).

[4] D. Haynes, Jr., D. Garber, C. Hooper, Jr., R. Mancini, Y. Lee, D. Bradley, J. Delettrez, R. Epstein, and P. Jaanimagi, Phys. Rev. E **53**, 1042 (1996).

[5] D. Bradley, J. Delettrez, R. Epstein, R. Town, C. Verdon, B. Yaakobi, S. Regan, F. Marshall, T. Boehly, J. Knauer, D. Meyerhofer, W. Seka, D. Haynes, Jr., M. Gunderson, G. Junkel, C. Hooper, Jr., P. Bell, and T. Ognibene, Physics of Plasmas **5**, 1870 (1998).

[6] C. Keane, B. Hammel, D. Kania, J. Kilkenny, R. Lee, A. Osterheld, L. Suter, R. Mancini, C. Hooper, Jr., and N. Delamater, Phys. Fluids B **5**, 3328 (1993).

[7] C. Hooper, Jr., R. Mancini, D. Haynes, Jr., and D. Garber, in *Elementary Processes in Dense Plasmas*, edited by S. Ichimaru and S. Ogata (Addison-Wesley, Reading, MA, 1995).

[8] H. Nishimura, T. Kiso, H. Shiraga, T. Endo, K. Fujita, A. Sunahara, H. Takabe, Y. Kato, and S. Nakai, Phys. Plasmas **2**, 2063 (1995).

[9] C. Hooper, Jr., Phys. Rev. **149**, 77 (1966).

[10] E. Smith and C. Hooper, Jr., Phys. Rev. **157**, 126 (1967).

[11] J. O'Brien and C. Hooper, Jr., J. Quant. Spectrosc. Radiat. Transfer **14**, 479 (1974).

[12] R. Tighe, *A Study of Stark Broadening of High-Z Hydrogenic Ion Lines in Dense Hot Plasmas*, Ph.D. thesis, University of Florida, 1977.

[13] R. Tighe and C. Hooper, Jr., Phys. Rev. A **14**, 1514 (1976).

[14] L. Woltz, *Stark Broadening in Laser-Produced Plasmas: Full Coulomb Calculation*, Ph.D. thesis, University of Florida, 1982.

[15] L. Woltz and C. Hooper, Jr., Phys. Rev. A **30**, 468 (1984).

[16] H. Griem, M. Blaha, and P. Kepple, Phys. Rev. A **41**, 5600 (1990).

[17] H. Nguyen, M. Koenig, D. Benredjem, M. Caby, and G. Coulaud, Phys. Rev. A **33**, 1279 (1986).

[18] G. Junkel, *Second-order, Full-Coulomb Electron Broadening Calculations for Multi-electron Radiators in Hot, Dense Plasmas: A Focus on Dense Plasma Line Shifts*, Ph.D. thesis, University of Florida, 2000.

[19] G. Junkel, M. Gunderson, C. Hooper, Jr., and D. Haynes, Jr., Phys. Rev. E **62**, 305 (2000).

[20] R. Tighe and C. Hooper, Jr., Phys. Rev. A **17**, 410 (1978).

[21] E. Smith, C. Vidal, and J. Cooper, J. Res. Nat. Bur. Stand (U.S.) **73A**, 389 (1969).

[22] E. Smith, C. Vidal, and J. Cooper, J. Res. Nat. Bur. Stand (U.S.) **73A**, 405 (1969).

[23] E. Smith, J. Cooper, and C. Vidal, Phys. Rev. **185**, 405 (1969).

[24] C. Vidal, J. Cooper, and E. Smith, J. Quant. Spectrosc. Radiat. Transfer **10**, 1011 (1970).

[25] R. Greene, J. Cooper, and E. Smith, J. Quant. Spectrosc. Radiat. Transfer **15**, 1025 (1975).

[26] R. Greene and J. Cooper, J. Quant. Spectrosc. Radiat. Transfer **15**, 1037 (1975).

[27] R. Greene and J. Cooper, J. Quant. Spectrosc. Radiat. Transfer **15**, 1045 (1975).

[28] G. Chiu and A. Ng, Phys. Rev. E **59**, 1024 (1999).

[29] M. Dharma-wardana and F. Perrot, Phys. Rev. A **45**, 5883 (1992).

[30] R. More, Advances in Atomic and Molecular Physics **21**, 305 (1985).

[31] D. Mihalas, *Stellar Atmospheres* (W.H. Freemen and Company, New York, NY, 1978).

[32] J. Ward, J. Cooper, and E. Smith, J. Quant. Spectrosc. Radiat. Transfer **14**, 555 (1974).

[33] E. Smith, J. Cooper, W. Chappell, and T. Dillon, J. Quant. Spectrosc. Radiat. Transfer **11**, 1547 (1971).

[34] E. Smith, J. Cooper, W. Chappell, and T. Dillon, J. Quant. Spectrosc. Radiat. Transfer **11**, 1567 (1971).

[35] L. Woltz and C. Hooper, Jr., Phys. Rev. A **38**, 4766 (1988).

[36] D. Boercker and C. Iglesias, Phys. Rev. A **30**, 468 (1984).

[37] D. Kilcrease, R. Mancini, and C. Hooper, Jr., Phys. Rev. E **48**, 3901 (1993).

[38] D. Boercker, C. Iglesias, and J. Dufty, Phys. Rev. A **36**, 2254 (1987).

[39] T. Hussey, J. Dufty, and C. Hooper, Jr., Phys. Rev. A **16**, 1248 (1977).

[40] H. Minoo, M. M. Gombert, and C. Deutsch, Phys. Rev. A **23**, 924 (1981).

[41] E. Wigner, A. Phyzik **43**, 624 (1927).

[42] C. Eckart, Rev. Mod. Phys **2**, 305 (1930).

[43] R. Cowan, *The Theory of Atomic Structure and Spectra* (University of California Press, Berkeley, CA, 1981).

[44] R. Mancini, D. Kilcrease, L. Woltz, and C. Hooper, Jr., Comp. Phys. Comm. **63**, 314 (1991).

[45] J. Cooper, D. Kelleher, and R. Lee, in *Proceedings of the 2nd International Conference on the Radiative Properties of Hot Dense Matter*, edited by J. Davis, C. Hooper, R. Lee, A. Merts, and B. Rozsnyai (World Scientific Press, Singapore, 1985).

[46] R. Zwanzig, in *Lectures in Theoretical Physics*, edited by W. Brittin, B. Downs, and J. Downs (Interscience Publishers, Inc., New York, NY, 1960), Vol. 3.

[47] C. Iglesias and J. Dufty, in *Spectral Line Shapes*, edited by K. Burnett (Walter de Gruyter and Co., New York, NY, 1983), Vol. 2.

[48] E. Wigner, in *Quantum Theory of Angular Momentum*, edited by L. Biedenharn and H. van Dam (Academic Press, New York, NY, 1965).

[49] A. Edmonds, *Angular Momentum in Quantum Mechanics* (Princeton University Press, Princeton, NJ, 1960).

BIOGRAPHICAL SKETCH

Mark Allen Gunderson was born February 28, 1969, in Monticello, Minnesota. He graduated from Central Valley Public School, Buxton, North Dakota, in May 1987. He attended the University of North Dakota in Grand Forks, where he received the degree of Bachelor of Science in physics in May 1991. He also attended graduate school at the University of North Dakota and received the degree of Master of Science in physics in August 1993. From August 1993 until December 2001, he was a graduate student in the Department of Physics at the University of Florida.

I certify that I have read this study and that in my opinion it conforms to acceptable standards of scholarly presentation and is fully adequate, in scope and quality, as a dissertation for the degree of Doctor of Philosophy.

Charles F. Hooper, Jr., Chairman
Professor of Physics

I certify that I have read this study and that in my opinion it conforms to acceptable standards of scholarly presentation and is fully adequate, in scope and quality, as a dissertation for the degree of Doctor of Philosophy.

James W. Dufty
Professor of Physics

I certify that I have read this study and that in my opinion it conforms to acceptable standards of scholarly presentation and is fully adequate, in scope and quality, as a dissertation for the degree of Doctor of Philosophy.

David B. Tanner
Distinguished Professor of Physics

I certify that I have read this study and that in my opinion it conforms to acceptable standards of scholarly presentation and is fully adequate, in scope and quality, as a dissertation for the degree of Doctor of Philosophy.

David H. Reitze
Associate Professor of Physics

I certify that I have read this study and that in my opinion it conforms to acceptable standards of scholarly presentation and is fully adequate, in scope and quality, as a dissertation for the degree of Doctor of Philosophy.

Stephen T. Gottesman
Professor of Astronomy

This dissertation was submitted to the Graduate Faculty of the Department of Physics in the College of Liberal Arts and Sciences and to the Graduate School and was accepted as partial fulfillment of the requirments for the degree of Doctor of Philosophy.

December 2001

Dean, Graduate School